55. Matilainen H, Makela AR, Riikonen R *et al.*: RGD motifs on the surface of baculovirus enhance transduction of human lung carcinoma cells. *J. Biotechnol.* 125, 114–126 (2006).
56. Ernst W, Schinko T, Spenger A, Oker-Blom C, Grabherr R: Improving baculovirus transduction of mammalian cells by surface display of a RGD-motif. *J. Biotechnol.* 126, 237–240 (2006).
57. Makela AR, Matilainen H, White DJ, Ruoslahti E, Oker-Blom C: Enhanced baculovirus-mediated transduction of human cancer cells by tumor-homing peptides. *J. Virol.* 80, 6603–6611 (2006).
58. Kafri T: Gene delivery by lentivirus vectors an overview. *Methods Mol. Biol.* 246, 367–390 (2004).
59. Lichty BD, Power AT, Stojdl DF, Bell JC: Vesicular stomatitis virus: re-inventing the bullet. *Trends Mol. Med.* 10, 210–216 (2004).
60. Hefferon KL, Oomens AG, Monsma SA, Finnerty CM, Blissard GW: Host cell receptor binding by baculovirus GP64 and kinetics of virion entry. *Virology* 258, 455–468 (1999).
61. Oomens AG, Blissard GW: Requirement for GP64 to drive efficient budding of *Autographa californica* multicapsid nucleopolyhedrovirus. *Virology* 254, 297–314 (1999).
62. Lung O, Westenberg M, Vlak JM, Zuidema D, Blissard GW: Pseudotyping *Autographa californica* multicapsid nucleopolyhedrovirus (AcMNPV): F proteins from group II NPVs are functionally analogous to AcMNPV GP64. *J. Virol.* 76, 5729–5736 (2002).
63. Mangor JT, Monsma SA, Johnson MC, Blissard GW: A GP64-null baculovirus pseudotyped with vesicular stomatitis virus G protein. *J. Virol.* 75, 2544–2556 (2001).
64. Aoki H, Sakoda Y, Jukuroki K, Takada A, Kida H, Fukusho A: Induction of antibodies in mice by a recombinant baculovirus expressing pseudorabies virus glycoprotein B in mammalian cells. *Vet. Microbiol.* 68, 197–207 (1999).
65. Facciabene A, Aurisicchio L, La Monica N: Baculovirus vectors elicit antigen-specific immune responses in mice. *J. Virol.* 78, 8663–8672 (2004).
66. Yoshida S, Kondoh D, Arai E *et al.*: Baculovirus virions displaying *Plasmodium berghei* circumsporozoite protein protect mice against malaria sporozoite infection. *Virology* 316, 161–170 (2003).
67. Strauss R, Huser A, Ni S *et al.*: Baculovirus-based vaccination vectors allow for efficient induction of immune responses against *Plasmodium falciparum* circumsporozoite protein. *Mol. Ther.* 15, 193–202 (2007).
68. Kaba SA, Nene V, Musoke AJ, Vlak JM, van Oers MM: Fusion to green fluorescent protein improves expression levels of *Theileria parva* sporozoite surface antigen p67 in insect cells. *Parasitology* 125, 497–505 (2002).
69. Rahman MM, Shaila MS, Gopinathan KP: Baculovirus display of fusion protein of *Peste des petits ruminants* virus and hemagglutination protein of *Rinderpest* virus and immunogenicity of the displayed proteins in mouse model. *Virology* 317, 36–49 (2003).
70. Tami C, Peralta A, Barbieri R, Berinstein A, Carrillo E, Taboga O: Immunological properties of FMDV-gP64 fusion proteins expressed on SF9 cell and baculovirus surfaces. *Vaccine* 23, 840–845 (2004).
71. Yang DG, Chung YC, Lai YK, Lai CW, Liu HJ, Hu YC: Avian influenza virus hemagglutinin display on baculovirus envelope: cytoplasmic domain affects virus properties and vaccine potential. *Mol. Ther.* 15, 989–996 (2007).
72. Akira S, Takeda K: Toll-like receptor signalling. *Nat. Rev. Immunol.* 4, 499–511 (2004).
73. Hemmi H, Takeuchi O, Kawai T *et al.*: A Toll-like receptor recognizes bacterial DNA. *Nature* 408, 740–745 (2000).
74. Hervas-Stubbs S, Rueda P, Lopez L, Leclerc C: Insect baculoviruses strongly potentiate adaptive immune responses by inducing type I IFN. *J. Immunol.* 178, 2361–2369 (2007).
75. Park SW, Lee HK, Kim TG, Yoon SK, Paik SY: Hepatocyte-specific gene expression by baculovirus pseudotyped with vesicular stomatitis virus envelope glycoprotein. *Biochem. Biophys. Res. Commun.* 289, 444–450 (2001).
76. Delaney WEt, Isom HC: Hepatitis B virus replication in human HepG2 cells mediated by hepatitis B virus recombinant baculovirus. *Hepatology* 28, 1134–1146 (1998).
77. Kitajima M, Hamazaki H, Miyano-Kurosaki N, Takaku H: Characterization of baculovirus *Autographa californica* multiple nuclear polyhedrosis virus infection in mammalian cells. *Biochem. Biophys. Res. Commun.* 343, 378–384 (2006).
78. Gao H, Wang Y, Li N *et al.*: Efficient gene delivery into mammalian cells mediated by a recombinant baculovirus containing a whispovirus IE1 promoter, a novel shuttle promoter between insect cells and mammalian cells. *J. Biotechnol.* 131, 138–143 (2007).
79. Condreay JP, Witherspoon SM, Clay WC, Kost TA: Transient and stable gene expression in mammalian cells transduced with a recombinant baculovirus vector. *Proc. Natl Acad. Sci. USA* 96, 127–132 (1999).
80. Ojala K, Mottershead DG, Suokko A, Oker-Blom C: Specific binding of baculoviruses displaying gp64 fusion proteins to mammalian cells. *Biochem. Biophys. Res. Commun.* 284, 777–784 (2001).
81. Ojala K, Koski J, Ernst W, Grabherr R, Jones I, Oker-Blom C: Improved display of synthetic IgG-binding domains on the baculovirus surface. *Technol. Cancer Res. Treat.* 3, 77–84 (2004).

Affiliations

- *Hideki Tani, PhD*
  Osaka University, Department of Molecular Virology, Research Institute for Microbial Diseases, Osaka, Japan
  Tel.: +81 668 798 343;
  Fax: +81 668 798 269;
  htani@biken.osaka-u.ac.jp
- *Takayuki Abe, PhD*
  Osaka University, Department of Molecular Virology, Research Institute for Microbial Diseases, Osaka, Japan
  Tel.: +81 668 798 343;
  Fax: +81 668 798 269;
  atakayu@biken.osaka-u.ac.jp
- *Tomoko M Matsunaga, PhD*
  Osaka University, Department of Molecular Virology, Research Institute for Microbial Diseases, Osaka, Japan
  Tel.: +81 668 798 343;
  Fax: +81 668 798 269;
  mtomo@biken.osaka-u.ac.jp
- *Kohji Moritishi, DVM, PhD*
  Osaka University, Department of Molecular Virology, Research Institute for Microbial Diseases, Osaka, Japan
  Tel.: +81 668 798 343;
  Fax: +81 668 798 269;
  kohji@biken.osaka-u.ac.jp
- *Yoshiharu Matsuura, DVM, PhD*
  Osaka University, Department of Molecular Virology, Research Institute for Microbial Diseases, 3-1 Yamada-oka, Suita, Osaka 565-0871, Japan
  Tel.: +81 668 798 340;
  Fax: +81 668 798 269;
  matsuura@biken.osaka-u.ac.jp

Available online at www.sciencedirect.com
ScienceDirect
VIROLOGY
ELSEVIER
Virology xx (2008) xxx – xxx
www.elsevier.com/locate/yviro

Crystal structure of the catalytic domain of Japanese encephalitis virus NS3 helicase/nucleoside triphosphatase at a resolution of 1.8 Å

Tetsuo Yamashita [a], Hideaki Unno [b], Yoshio Mori [a], Hideki Tani [a], Kohji Moriishi [a], Akihisa Takamizawa [c], Masanobu Agoh [d], Tomitake Tsukihara [e], Yoshiharu Matsuura [a,*]

[a] *Department of Molecular Virology, Research Institute for Microbial Diseases, Osaka University, Osaka, Japan*
[b] *Department of Applied Chemistry, Faculty of Engineering, Nagasaki University, Nagasaki, Japan*
[c] *Kanonji Institute, The Research Foundation for Microbial Diseases of Osaka University, Kagawa, Japan*
[d] *Nagasaki Prefectural Institute for Environmental Research and Public Health, Nagasaki, Japan*
[e] *Department of Protein Crystallography, Research Institute for Protein Research, Osaka University, Osaka, Japan*

Received 31 October 2007; returned to author for revision 20 November 2007; accepted 11 December 2007

Abstract

The NS3 protein of Japanese encephalitis virus (JEV) is a large multifunctional protein possessing protease, helicase, and nucleoside 5′-triphosphatase (NTPase) activities, and plays important roles in the processing of a viral polyprotein and replication. To clarify the enzymatic properties of NS3 protein from a structural point of view, an enzymatically active fragment of the JEV NTPase/helicase catalytic domain was expressed in bacteria and the crystal structure was determined at 1.8 Å resolution. JEV helicase is composed of three domains, displays an asymmetric distribution of charges on its surface, and contains a tunnel large enough to accommodate single-stranded RNA. Each of the motifs I (Walker A motif), II (Walker B motif) and VI was composed of an NTP-binding pocket. Mutation analyses revealed that all of the residues in the Walker A motif (Gly^{199}, Lys^{200} and Thr^{201}), in addition to the polar residues within the NTP-binding pocket (Gln^{457}, Arg^{461} and Arg^{464}), and also Arg^{458} in the outside of the pocket in the motif IV were crucial for ATPase and helicase activities and virus replication. Lys^{200} was particularly indispensable, and could not be exchanged for other amino acid residues without sacrificing these activities. The structure of the NTP-binding pocket of JEV is well conserved in dengue virus and yellow fever virus, while different from that of hepatitis C virus. The detailed structural comparison among the viruses of the family *Flaviviridae* should help in clarifying the molecular mechanism of viral replication and in providing rationale for the development of appropriate therapeutics.

Keywords: JEV; NTPase/helicase; Crystal structure; Replication

Introduction

The genus *Flavivirus* within the family *Flaviviridae* contains many arthropod-borne viruses, such as Japanese encephalitis virus (JEV), West Nile virus (WNV), dengue virus (DEN), yellow fever virus (YFV) and tick-borne encephalitis virus. JEV is still one of the most important flaviviruses in medical and veterinary fields despite the wide availability of inactive vaccines. JEV is distributed in the south and southeast regions of Asia and kept in a zoonotic transmission cycle between pigs or birds and mosquitoes (Solomon et al., 2003; Tsai, 2000). JEV spreads to dead-end hosts, including humans, through the bite of mosquitoes infected with JEV and causes infection of the central nervous system, with a high mortality rate. JEV has a plus-sense single-stranded RNA genome approximately 11 kb in length, which is capped at the 5′ end but lacks modification of the 3′ terminus by polyadenylation. The genome is translated into a single precursor polyprotein which is subsequently processed by host and viral proteases to produce three structural proteins, C, prM and E, and seven non-structural proteins, NS1, NS2A, NS2B, NS3, NS4A, NS4B and NS5 (Sumiyoshi et al.,

* Corresponding author. Department of Molecular Virology, Research Institute for Microbial Diseases, Osaka University, 3-1 Yamadaoka, Suita-shi, Osaka 565-0871, Japan. Fax: +81 6 6879 8269.
E-mail address: matsuura@biken.osaka-u.ac.jp (Y. Matsuura).

0042-6822/$ - see front matter © 2008 Elsevier Inc. All rights reserved.
doi:10.1016/j.virol.2007.12.018

1987). NS3 is a multifunctional protein of 619 amino acid residues. The N-terminal one-third of NS3 has a serine protease activity that participates in the processing together with a co-factor protein NS2B. The NS3 protein also has a catalytic domain for helicase, nucleoside 5′-triphosphatase (NTPase), as well as 5′-terminal RNA triphosphatase activities in the C-terminal two-thirds. Functionally, the enzymatic activities of helicase and ATPase have been confirmed in the NS3 proteins derived from several members of the family *Flaviviridae*, including viruses from the genus *Flavivirus*, such as JEV, DEN, YFV, and from the genus *Hepacivirus*, such as hepatitis C virus (HCV) (Cui et al., 1998; Kuo et al., 1996; Li et al., 1999b; Warrener et al., 1993; Wengler and Wengler, 1991). Although the precise biological functions of the helicase/NTPase domain are unclear, one possible explanation is that the domain may resolve double-stranded RNA intermediates formed during transcription or replication of genomic RNA. The DEN mutants impaired in NTPase and helicase activities displayed little or no replication (Matusan et al., 2001), suggesting that flaviviral helicase/NTPase is essential for the viral life cycle and could be an ideal target for the development of antiviral drugs.

Helicases are motor enzymes that use energy derived from NTP hydrolysis to catalyze the unwinding and remodeling of double-stranded nucleic acids, and they are classified into three superfamilies based on sequence comparison and conserved motifs (Luking et al., 1998). Helicase can be further classified into DEAD, DExD, and DExx subfamilies based on the sequence of motif II (Ahmadian et al., 1997; Luking et al., 1998; Schmid and Linder, 1992). All helicases bind NTP using two structural elements, the motif I/Walker A motif, which is a phosphate-binding P-loop, and the motif II/Walker B motif, which is a Mg^{2+}-binding aspartic acid loop (Koonin, 1991). NS3 helicases of flaviviruses and HCV are classified into superfamily 2 (Kim et al., 1997; Utama et al., 2000a,b). Superfamily 2 RNA helicases, also called DEA(D/H)-box helicases after the signature sequence in the Walker B motif, have seven conserved motifs, and these motifs are suggested to be associated with NTP hydrolysis and nucleic acid binding (Fig. 1A). Recently, a conserved Q motif upstream of the Walker A motif was reported to be essential for the ATPase activity of DEAD-box helicases (Tanner et al., 2003). Utama et al. have shown that the motif II (DExH/D) of both JEV and HCV NS3 proteins is essential for RNA helicase and ATPase activities (Utama et al., 2000a,b). The crystal structures have been reported for several helicases, including the DNA helicase PcrA from *Bacillius stearothermophilus* (Subramanya et al., 1996) and Rep from *Escherichia coli* (*E.coli*) (Korolev et al., 1997) of the superfamily 1 and the NS3 helicases from DEN, YFV, and HCV (Cho et al., 1998; Kim et al., 1998; Yao et al., 1997; Yao et al.,

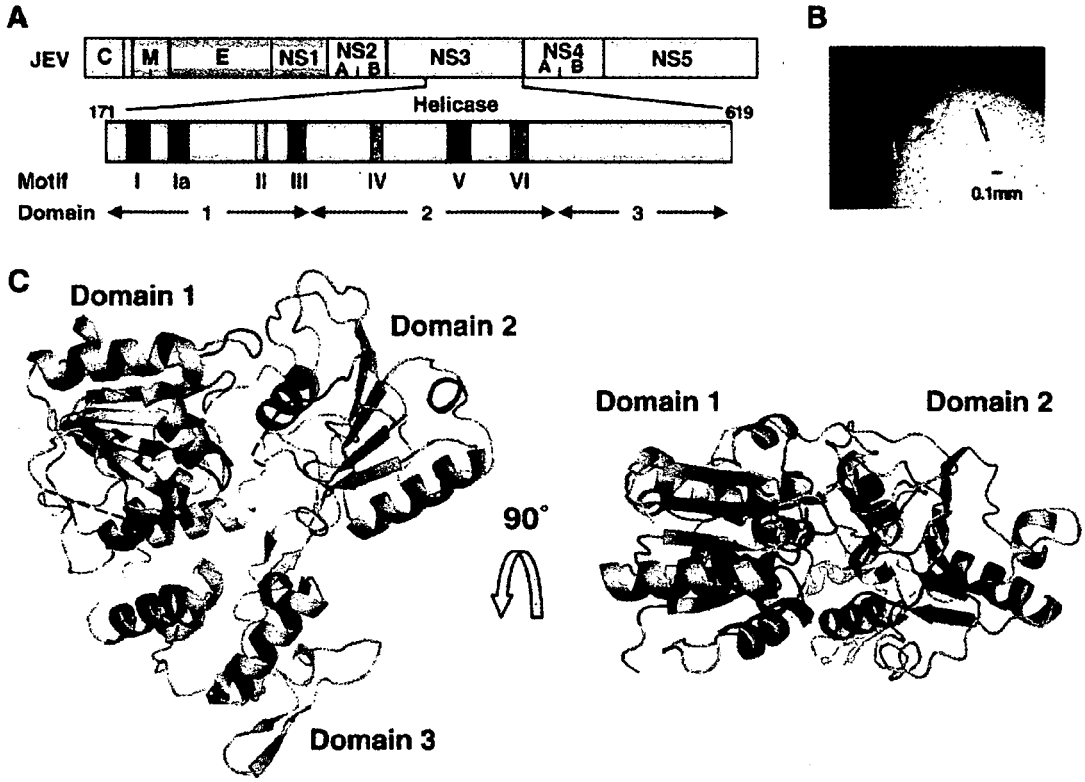

Fig. 1. Genome structure of JEV, crystals of JEV NS3 helicase/NTPase, and the three-dimensional structure. (A) Genome structure of JEV and the seven conserved motifs in JEV helicase domain. (B) Crystals of JEV NS3 helicase/NTPase domain obtained in the drop after 5 days of incubation. (C) The ribbon diagram of the JEV NS3 helicase/NTPase domain shows domain 1 and 2 at the top and domain 3 at the bottom (left). The seven helicase motifs are colored separately (motif I, purple; motif Ia, red; motif II, cyan; motif III, orange; motif IV, pink; motif V, blue; motif VI, green). Two regions, 245–252 and 413–415, are disordered and displayed as a broken line. The upper view of the JEV helicase/NTPase domain is shown at right.

Please cite this article as: Yamashita, T., et al., Crystal structure of the catalytic domain of Japanese encephalitis virus NS3 helicase/nucleoside triphosphatase at a resolution of 1.8 Å, Virology (2008), doi:10.1016/j.virol.2007.12.018

1999) and UvrB from *Bacillus caldotenax* (Theis et al., 1999), which are members of the superfamily 2. These structural studies revealed that the helicase motifs constitute an NTPase activity site at the interface of two domains and that a cleft between these two domains and a third is a binding site for single-stranded nucleic acids, suggesting that the same mechanisms underlie NTP hydrolysis and strand unwinding. However, Borowski et al. have shown that the inhibitory effects of halogenated benzimidazole and benzotriazole derivatives against NTPase and the helicase activities of NS3 proteins varied among JEV, WNV and HCV, suggesting that the enzymatic active sites of these viruses are structurally different (Borowski et al., 2003).

In this study, we examined a refined three-dimensional structure of the JEV helicase/NTPase domain. The three-lobed structure displays an asymmetric distribution of charges on its surface and contains a tunnel large enough to accommodate single-stranded RNA. The overall structure is similar to other flavivirus helicases (Wu et al., 2005; Xu et al., 2005; Yao et al., 1997) and each of the motifs I, II and VI is composed of an NTP-binding pocket. Mutation analyses revealed that the residues in the Walker A motif and the motif VI were crucial for not only ATPase and helicase activities but also virus replication. The detailed structural comparison among members of the family *Flaviviridae* should provide further insight into the molecular mechanisms of viral RNA replication.

Results

Overall structure

The structure of the JEV helicase/NTPase domain (amino acid residues 171 to 619) was determined using the molecular replacement method based on data collected at 1.8 Å resolution. A summary of the data collection, phasing, density modification and structure refinement statistics is shown in Table 1. JEV NS3 helicase is composed of three domains of roughly equal size with DEN, YFV and HCV helicases (Fig. 1C). Like other helicases, each domain 1 or 2 of the JEV helicase forms an α/β domain with a RecA-like topology. The available structures suggest that nucleic acids bind across the interface of two RecA-like fold domains (Velankar et al., 1999). Domain 1 (amino acid residues 171–328) is composed of four α-helices and five β-sheets. The cluster of the β-strands is surrounded by three of the four α-helices. The seven sequence motifs of superfamily 2 helicases (Koonin, 1991) were assigned to domains 1 and 2 (Fig. 1A). Domain 1 has two ATP-binding motifs, Walker A (motif I; GSGKT) and Walker B (motif II; DEAH), which are conserved among three helicase superfamilies. Domain 2 (amino acid residues 329–482) is composed of three α-helices and eight β-strands and divided into two subunits. One subunit is surrounded by six β-strands and three α-helices, and the other has two β-strands penetrating into domain 3. The motifs Ia, II and V face each other across the domain boundary and participate in a tight configuration. An arginine finger in motif VI (QRRGRVGR) in domain 2 is thought to be crucial for NTP hydrolysis (Ahmadian et al., 1997; Caruthers and McKay, 2002; Niedenzu et al., 2001). Domain 3 (amino acid residues 483–619) is composed of seven α-helices and two β-strands.

Table 1
Data collection and refinement statistics

Diffraction data	
X-ray source	SPring-8 BL44-XU
Detector	Mac Science DIP6040
Temperature (K)	100
Space group	$P2_1$
Unit–cell parameters	
a (Å)	59.31
b (Å)	68.31
c (Å)	65.48
β (°)	116.89
X-ray wavelength (Å)	0.9000
Resolution range (Å)	50–1.80 (1.86–1.80)
Total reflections	83514 (8266)
Multiplicity	4.2 (4.2)
R_{merge} [a]	0.051 (0.434)
Completeness (%)	99.9 (99.5)
I/sigma I	20.8 (3.8)
Refinement statistics	
Resolution range (Å)	20–1.8
Unique reflections	42747 (4264)
R (%)	19.7
R_{free} (%)	24.7
RMSD bond length (Å)	0.016
RMSD bond angle (Å)	1.611
Water molecules (no.)	413

Values in square brackets refer to the highest resolution shell.
[a] $R_{merge} = \Sigma_{hkl}\Sigma_i|I(hkl)_i - \langle I(hkl)/\Sigma_{hkl}I(hkl)\rangle|$, where $I(hkl)_i$ is the *i*th measurement of the intensity of reflection *hkl* and $\langle I(hkl)\rangle$ is the mean intensity of reflection *hkl*.

NTP-binding region

To examine the ATP-binding state of the JEV helicase, a hypothetical ATP-binding model was built (Fig. 2). The model showed that an ATP molecule was localized with the cleft between domains 1 and 2 (Fig. 2A). In the ATP-binding pocket formed by the cleft, an ATP molecule was associated with the Walker A motif (motif I), Walker B motif (motif II), and motif VI (Fig. 2B). All residues in these motifs were well conserved among the DEAH-box helicase proteins (Schmid and Linder, 1992). Based on the crystal structure of JEV helicase, positively charged residues, Lys^{200}, Arg^{461} and Arg^{464} are present in the pocket of the active sites of motifs I, II and VI. Lys^{200} protrudes into the pocket, recognizes the β-or γ-phosphate of ATP and forms a salt bridge with Asp^{285} and Glu^{286} for stabilization of the active site structure. Arg^{461} and Arg^{464} in motif VI form an arginine finger, work as sensors recognizing the γ-and α-phosphate of ATP, and are critical for conformational switching upon ATP hydrolysis (Ahmadian et al., 1997; Caruthers and McKay, 2002; Niedenzu et al., 2001). One water is coordinated with residues Glu^{286}, His^{288} and Gln^{457} at distances of 2.73 Å, 2.67 Å and 4.0 Å, respectively. His^{288} is essential for RNA-unwinding activity (Utama et al., 2000a,b).

Nucleic acid-binding site

The domain 3 of JEV helicase interacts with domains 1 and 2 to form a groove at the domain boundary (Fig. 3). Among the

Please cite this article as: Yamashita, T., et al., Crystal structure of the catalytic domain of Japanese encephalitis virus NS3 helicase/nucleoside triphosphatase at a resolution of 1.8 Å, Virology (2008), doi:10.1016/j.virol.2007.12.018

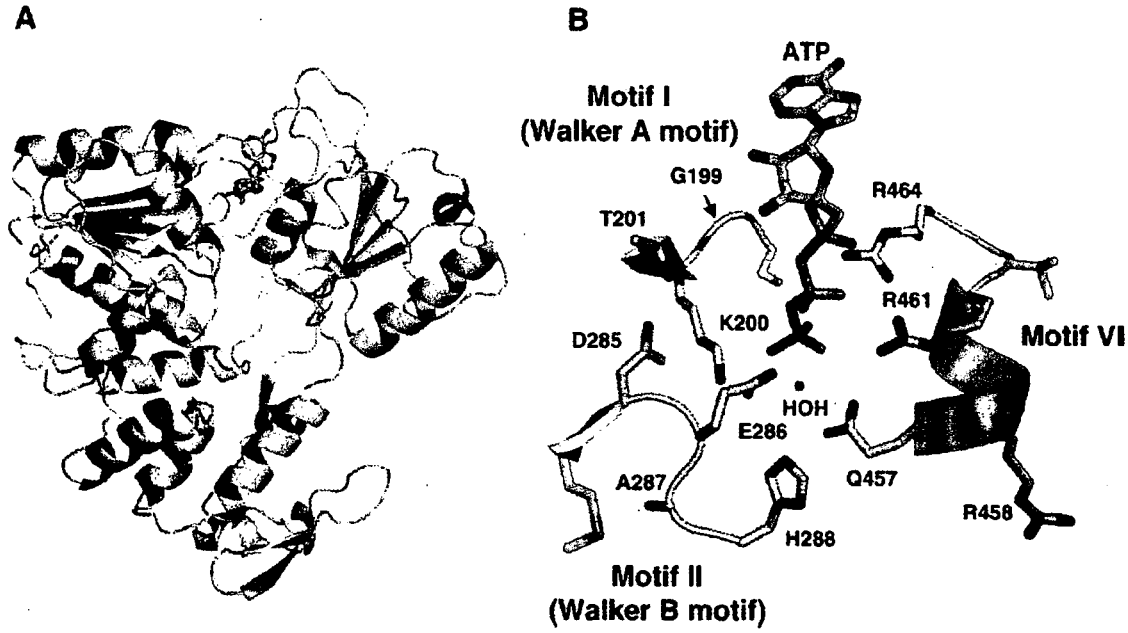

Fig. 2. A hypothetical ATP-binding model of the JEV helicase/NTPase. (A) Overall structure of the JEV helicase/NTPase domain with an ATP molecule. Orientation of the structure is identical with the Fig. 1C. The ATP molecule is localized in the cleft between the domains 1 and 2. (B) An ATP-binding pocket formed by the motifs I, II and IV. The residues consist of the ATP-binding pocket are indicated by colored atoms (C, gray; N, blue; O, red). An ATP molecule is indicated by colored atoms (C, green; N, blue; O, red; P, orange). Lys^{200} recognizes β-or γ -phosphate of ATP and forms a salt bridge with Asp^{285} and Glu^{286} for stabilization of the active site structure. Arg^{461} and Arg^{464} in motif VI form an arginine finger, work as sensors recognizing the γ-, β- and α-phosphate of ATP, respectively. The water molecule is coordinated by residues Glu^{286}, His^{288} and Gln^{457}. His^{288} is essential for the RNA-unwinding activity.

members of the family *Flaviviridae*, the structure of HCV helicase has been resolved as a helicase–nucleic acid complex (Kim et al., 1998), in which an oligomer (dU)8 is bound to the cleft between domain 3 and domains 1 and 2, with the 5′ and 3′ ends beneath the domains 2 and 1, respectively. The crystal structures of other helicases resolved with nucleic acids are superfamily 1 helicases PcrA and Rep in which a DNA duplex is bound along the side of the protein shared by domain 2 and the analog of domain 3 (Korolev et al., 1997; Velankar et al., 1999). Based on the common binding orientation in these complexes, we assumed that a single-stranded RNA proceeds through the major inter-domain cleft of the flavivirus helicase from the domain 2 side toward the domain 1 side of the protein. The structure of JEV helicase reveals that one surface has a rigid structure composed of α-helices and β-strands forming a long tunnel surrounded by residues emanating from the three domains that cross the center of the face, whereas the other surface is more negatively charged (Fig. 3). This tunnel is lined with a number of positively charged residues, with several basic patches able to accommodate a single-stranded nucleic acid, but not a duplex. JEV helicase contains an unusually high proportion of charged residues and the distribution of these residues on its surface is asymmetric just as in DEN, YFV and HCV (Wu et al., 2005; Xu et al., 2005; Yao et al., 1997). These data suggest that electrostatic repulsion might be involved in the RNA winding.

Comparison of flavivirus helicases

Previous structural analyses of the helicases of DEN, YFV, and HCV revealed that these viral helicases have highly similar structures consisting of three functional domains (Wu et al., 2005; Xu et al., 2005; Yao et al., 1997). The amino acid sequences of the NS3 helicase domain of JEV exhibited 65%, 44% and 23% homology to those of DEN, YFV and HCV, respectively. The crystal structures of the NS3 helicases of DEN (Xu et al., 2005) and YFV (Wu et al., 2005) are similar to that of JEV but slightly different from HCV (Yao et al., 1997). The distance between domains 1 and 2 of HCV helicase is longer than that in flavivirus NS3 helicases, indicating that the HCV helicase has an ATP-binding pocket with a larger volume than other flaviviruses, and the folding of domain 3 the HCV helicase is unique while that of JEV is very similar to those of other flaviviruses, including DEN and YFV (Fig. 4A). Superposition of JEV, DEN, YFV, and HCV helicases further clarified that the HCV helicase has a unique conformation in the NTPase-binding region and domain 3 in comparison with JEV, DEN, and YFV helicases (Fig. 4B). In particular, the conformation of motifs I and II of HCV helicase were different from that of JEV, DEN, and YFV helicases (Fig. 4C). The distance between motifs I and II of Cα of HCV and the other flaviviruses were 6.7 Å and 3.5 Å, respectively. The distance of Nz of Lys^{200} in the motif I was different in 4.7 Å between JEV and HCV, suggesting that HCV helicase has a wider ATP-binding pocket than other flaviviruses. In contrast to the structure of motifs I and II, that of motif VI was well conserved among the flavivirus helicases, including HCV. Although a subtle difference is observed, the ATP-binding residues in JEV, DEN, YFV, and HCV helicases are well conserved, suggesting that flavivirus helicases possess similar mechanisms of ATP hydrolysis.

Please cite this article as: Yamashita, T., et al., Crystal structure of the catalytic domain of Japanese encephalitis virus NS3 helicase/nucleoside triphosphatase at a resolution of 1.8 Å, Virology (2008), doi:10.1016/j.virol.2007.12.018

ATPase and RNA helicase activities

Amino acid residues in the motif II of JEV helicase have been already shown to be essential for RNA helicase activity (Utama et al., 2000a,b). To determine the biological significance of each amino acid residue in motifs I and VI of the JEV helicase in more detail, substitution mutants of the JEV helicase were prepared as shown in Fig. 5A. Structural analyses of helicases revealed that the amino group of Lys in the Walker A motif interacts with the phosphates of ATP and the hydroxyl of Thr or Ser in the same motif, and ligates a Mg^{2+}ion (Sengoku et al., 2006). A critical role of Gly and Lys in the Walker A motif in the enzymatic and/or biochemical functions has been reported in HCV and DEN helicases (Kim et al., 1997). First, to examine the role of Gly^{199}, Lys^{200} and Thr^{201} residues in the Walker A motif of the JEV helicase on the enzymatic activity, mutant JEV helicases, G199A, K200A and T201A, in which Ala was substituted for each amino acid residue, were prepared (Fig. 5B, left). All the mutants lost both the ATPase and helicase activities, suggesting that Gly^{199}, Lys^{200} and Thr^{201} are crucial for the enzymatic activity of JEV helicase (Fig. 5C and D). From the revealed structure of JEV helicase, it was suggested that an appropriate length of a side chain of Lys^{200} plays an important role in the electrostatic interaction with the substrate in NTP hydrolysis. To examine the role of the side chain of Lys^{200} on the enzymatic activity of JEV helicase, we constructed mutant JEV helicases, K200R, K200Q, K200N, K200D, K200E and K200H, in which the polar amino acid residues, Arg, Gln, Asn, Asp, Glu and His were substituted for Lys^{200} in the Walker A motif, respectively. Although SDS-PAGE analysis verified that the mutant helicase proteins had purities and loading quantities similar to the wild type helicase (Fig. 5B), neither ATPase nor RNA helicase activity was detected in the mutant proteins (Fig. 5C and D), suggesting that Lys^{200} in the ATP-binding pocket is an indispensable amino acid and plays a critical role in the enzymatic activity of JEV helicase by providing a side chain with an adequate charge and length to fit with the substrate.

The Arg^{461} and Arg^{464} within the arginine finger ($xR^{458}xG^{460}R^{461}xxR^{464}$) in the motif VI were suggested to be the active sites of ATP hydrolysis (Ahmadian et al., 1997). To further examine the role of the amino acid residues in the motif VI in ATP hydrolysis and RNA unwinding in more detail, we constructed a series of Ala substitution mutants, Q457A, R458A, R459A, G460A, R461A, V462A, G463A, and R464A (Fig. 5B, right). The R461A and R464A mutants completely lost ATPase activity and the Q457A and R458A mutants exhibited 80% and 90% reduction of ATPase activity, respectively (Fig. 5C), whereas all four of these mutants lost RNA helicase activity (Fig. 5D). These results suggest that Gln^{457}, Arg^{461} and Arg^{464} in the ATP-binding pocket participate in the enzymatic activities of JEV helicase by interacting with the substrate, and Arg^{458}, which is located outside of the ATP-binding pocket, may help to support the helix conformation of motif VI in an enzymatically active state. Although the conserved amino acid residues in the arginine finger were suggested to be essential for enzymatic activity, substitution of Ala for Gly^{460} had no effect on either ATPase or RNA-unwinding activities, as seen in the mutants in which non-conserved amino acid residues such as Gly^{463}, Val^{462} and Arg^{459} were substituted for Ala, suggesting that Gly^{460} does not play an important role in the enzymatic activity of JEV helicase. To

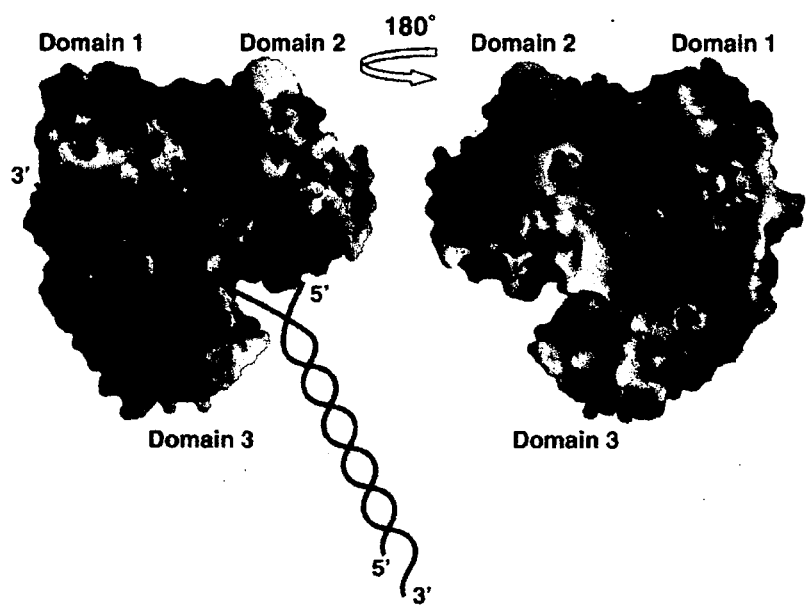

Fig. 3. Surface representation of the JEV NS3 helicase/NTPase domain. The left panel shows a nucleotide-binding face exhibiting a rigid structure composed of α-helices and β-strands and forming a long tunnel surrounded by residues emanating from the three domains that across the center of the face. Positive electrostatic potentials are colored blue and negative ones are colored red. The right panel provides a view of the other surface rotated by 180° around a vertical axis exhibiting a flat structure consisting of more negatively charged. The proposed binding groove for an RNA substrate (pink lines) is shown.

Please cite this article as: Yamashita, T., et al., Crystal structure of the catalytic domain of Japanese encephalitis virus NS3 helicase/nucleoside triphosphatase at a resolution of 1.8 Å, Virology (2008), doi:10.1016/j.virol.2007.12.018

further examine the effect of mutations in the helicase on the replication of JEV, we constructed full-length JEV genomic RNAs in which the amino acid residues in motifs I and VI were substituted. Mutations in the JEV helicase abrogating the enzymatic activities are lethal and no infectious virus was recovered (G199A, K200A, T201A, Q457A, R458A, R461A, and R464A) upon transfection of the full-length RNA into Vero cells, whereas infectious viruses were recovered upon transfection with RNA of the wild type and the G460A mutant possessing the enzymatic activities (data not shown). These results suggest that the amino acids in motifs I and VI participating in the ATPase/helicase activity are indispensable for viral replication as reported in DEN (Matusan et al., 2001).

Discussion

All viruses are thought to functionally require helicase for their replication. In general, most RNA viruses that replicate primarily in the cytoplasm carry a self-encoding helicase, whereas DNA viruses that replicate primarily in the nucleus often utilize a cellular helicase (Kwong et al., 2005). In this study we determined the crystal structure of the JEV NS3 helicase/NTPase domain and investigated the roles of the amino acids in the conserved sequence motifs on the enzymatic activities and virus replication. With respect to the overall structure, JEV helicase exhibited a three-dimensional structure that was similar to the DEN and YFV helicases, but was slightly different from that of the HCV helicase in the ATP-binding pocket and domain 3.

The motif I or Walker A motif is conserved in all three helicase superfamilies and involved in the binding to the β or γ phosphate group of NTPs. The motif II or Walker B motif is also present in all the superfamilies and predicted to bind to Mg^{2+}, forming a complex with the terminal phosphates of the NTPs. The signature NTP-binding sequence GSGKT, is located at the N-terminus of the α-helix in the Walker A motif and in close proximity to an invariant Asp localized within the DExH box in the Walker B motif. In the absence of substrate, the side chains of the Walker A and B motifs formed hydrogen bonds with each other and also with residues within a conserved TATPP sequence in the motif III. Interactions included a salt bridge between Lys and Asp side chains between Walker A and B

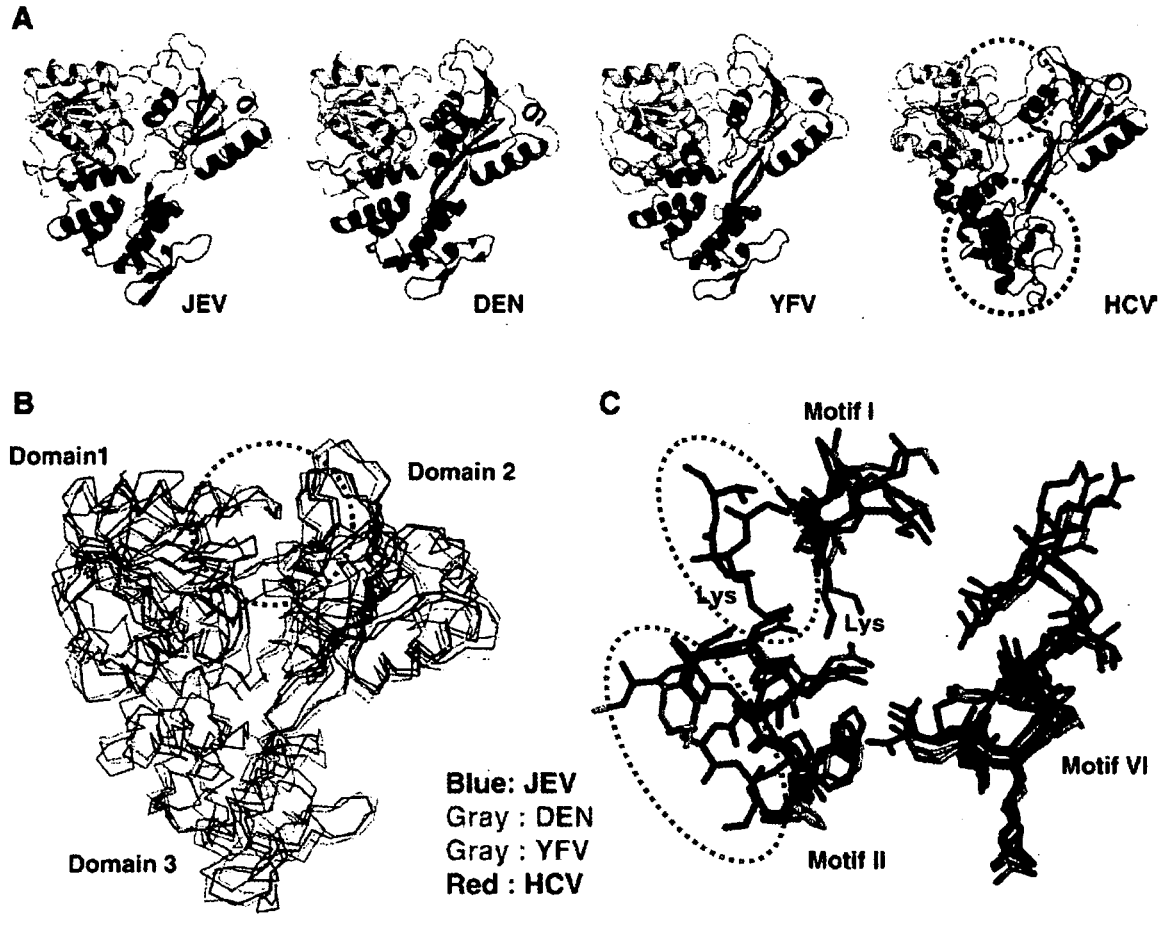

Fig. 4. Comparison of flavivirus NS3 helicase/NTPase domains. (A) Crystal structures of the NS3 helicase/NTPase domains of JEV, DEN (Protein Data Bank accession code 2BHR), YFV (Protein Data Bank accession code 1YKS) and HCV (Protein Data Bank accession code 1HEI). (B) Superimposition of each of helicase/NTPase domain. Gray: DEN and YFV; red: HCV; blue: JEV. (C) Superimposition of motifs I, II and VI. The side chains are indicated by colored atoms (C: gray; N: blue; O: red).

Please cite this article as: Yamashita, T., et al., Crystal structure of the catalytic domain of Japanese encephalitis virus NS3 helicase/nucleoside triphosphatase at a resolution of 1.8 Å, Virology (2008), doi:10.1016/j.virol.2007.12.018

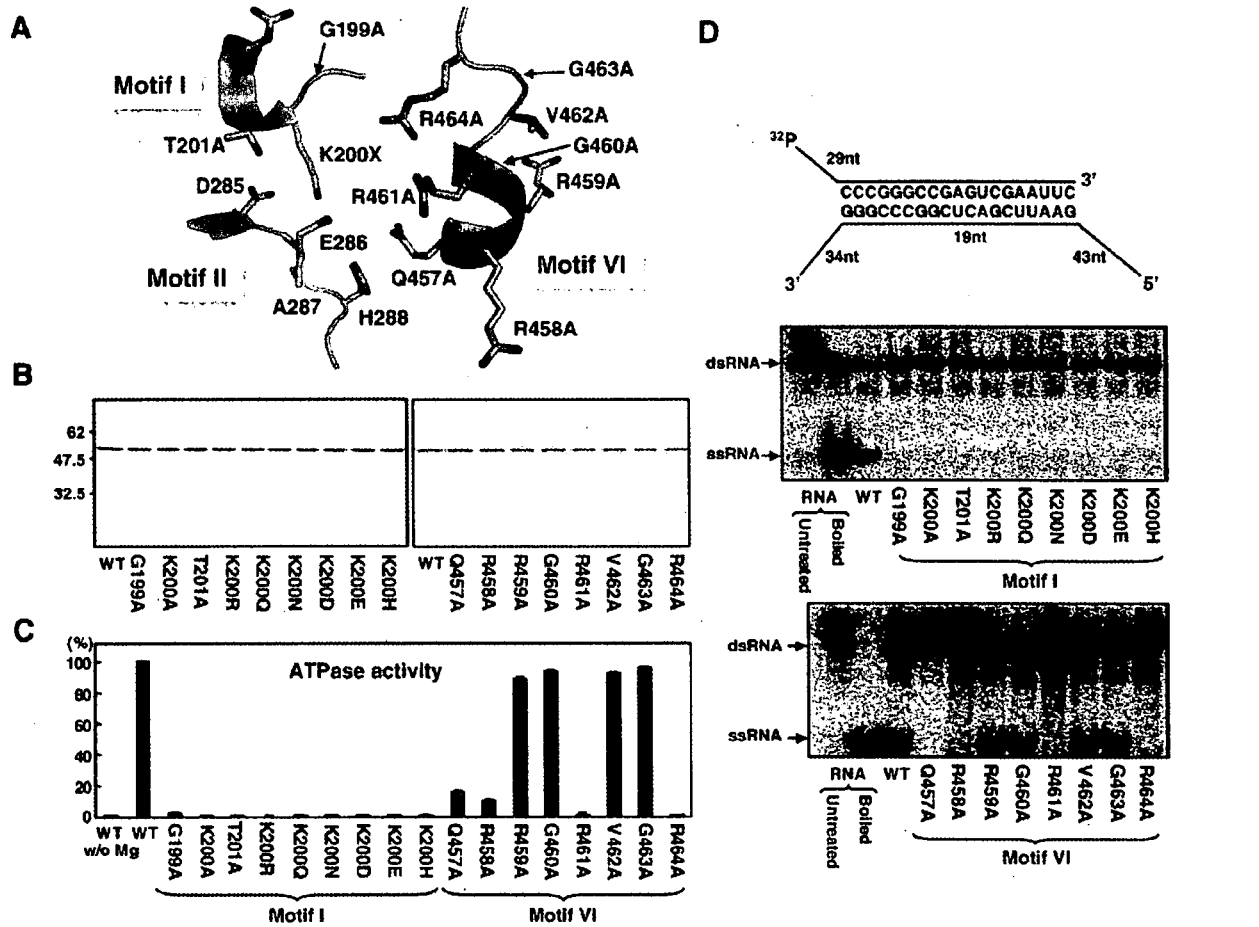

Fig. 5. ATPase and RNA helicase activities of the JEV NS3 helicase/NTPase domain. (A) Mutations introduced into amino acid residues of motif I (red) and motif VI (blue). (B) SDS-PAGE analysis of the purified JEV NS3 helicase/NTPase domain. One μg of the wild type or mutant proteins was subjected to SDS-PAGE and stained with Coomassie brilliant blue. The molecular mass of the JEV NS3 helicase/NTPase domain was about 54 kDa. (C) ATPase activities of the wild type and mutant proteins. The colorimetric NTPase assay was conducted by measuring the amount of free phosphate moiety release from nucleoside triphosphate as described in the Materials and methods. WT w/o Mg means ATPase activity of WT helicase in the absence of Mg^{2+}. The value obtained by using the wild type helicase is defined as 100%. (D) RNA helicase activities of wild type and mutant proteins. A schematic representation of the dsRNA substrate used in the unwinding assay is shown at the top of the figure. The representative images of RNA helicase assays are shown at the middle and bottom. The substrate dsRNA and unwinding ssRNA are indicated by arrows.

motifs. Structural comparisons identified the TATPP sequence located at the end of the β-strand between Walker A and B motifs and suggested that this sequence made up part of the 'switch region' responsible for the transition of conformational changes upon NTP hydrolysis (Kim et al., 1998).

Based on the crystal structure of JEV helicase, Lys^{200} is a polarity residue projecting into the ATP-binding pocket in motif I, suggesting that Lys^{200} interacts with β or γ-phosphate of ATP. We therefore constructed mutant helicases in which Lys^{200} was substituted for several other polarity residues. We speculated that a substitution of Lys^{200} for Arg retains the ATPase and RNA-unwinding activities, because both Lys and Arg are positively charged residues; however all mutants completely lost the enzymatic activities. These results suggest that Lys^{200} in motif I is indispensable for the activity due to its adequate polarity and sufficiently long side chain as well as its failure form a salt bridge with Asp^{285} and Glu^{286}. Although the other residues, Gly^{199} and Thr^{201}, in motif I do not have side chains to interact with the substrate, replacing these residues with Ala also abrogated the activity. In PcrA and Vasa, Thr in motif I was coordinated with Mg^{2+}(Sengoku et al., 2006; Velankar et al., 1999), suggesting that Gly^{199} and Thr^{201} in JEV helicase are important to sustain the conformation of the Walker A motif and that Mg^{2+}may be coordinated with Thr^{201} via an arrangement mediated by water.

The motif II or Walker B motif has a DEx(D/H) sequence known as the ATP-binding motif, and mutation analyses revealed that any residues would be accommodated in the *x* position (Marians, 1997). JEV helicase, a bovine diarrhea disease virus NS3 protein, HCV helicase, and *E. coli* UvrB have Ala, Tyr, Cys and Ser residues at the *x* position, respectively (Nakagawa et al., 1997). Previous mutational analyses in the DEAH motif of JEV helicase revealed that Asp^{285} and Glu^{286} in the motif were essential for both ATPase and RNA helicase activities, whereas Ala^{287} and His^{288} in the motif were indispensable for RNA helicase activity but not for ATPase activity (Utama et al.,

Please cite this article as: Yamashita, T., et al., Crystal structure of the catalytic domain of Japanese encephalitis virus NS3 helicase/nucleoside triphosphatase at a resolution of 1.8 Å, Virology (2008), doi:10.1016/j.virol.2007.12.018

2000a). Ala^{287} in the DEAH motif lacks a side chain interacting with substrate, and we therefore speculate that Asp^{285} coordinates Mg^{2+}via a mediating by water, and Asp^{285} and Ala^{287} are important to sustain the conformation of motif II by forming salt bridge with Lys^{200}. Although His^{288} is too far away to be considered an active site, our structural analyses suggest that His^{288} in the DEAH motif is required for helicase activity and plays a role in the NTP hydrolysis reaction by mediating the water.

The mutant JEV helicases in which Ala was substituted for Gln^{457}, Arg^{458}, Arg^{461} or Arg^{464} in the active site of motif VI, but not those in which Ala was substituted for Arg^{459}, Gly^{460}, Val^{462} or Gly^{463}, exhibited a drastic reduction in the ATPase and helicase activities. Mutations of Arg in the motif VI of HCV helicase completely abrogated both ATPase and helicase activities (Kim et al., 1997), and R457A and R458A mutants of DEN helicase retained the NTPase activity but lost the RNA-unwinding activity (Matusan et al., 2001). However, a full-length DEN NS3 mutant in which Ala was substituted for Arg^{457} and Arg^{458} exhibited a severe reduction in ATPase activity, but a two-fold increase in the helicase activity. The discrepancy in DEN helicase activity might be attributable to an approximately 30-fold higher activity in the full-length NS3 protein than in the N-terminally truncated helicase protein (Li et al., 1999a). Arg^{461} and Arg^{464} of JEV helicase interact with γ-and α -phosphate of ATP respectively, and Gln^{457} also interacts with γ-phosphate of ATP and coordinates water for NTPase hydrolysis with His^{288}. These results suggest that the arginine finger in motif VI of JEV helicase works as a sensor of substrate recognition and the binding pocket of NTPs plays an important role in the interaction with water, substrates and divalent cations.

The crystal structure of JEV helicase revealed a tunnel lined with a number of basic residues sufficient for accommodating a single-stranded nucleic acid. A conserved Trp^{501} in domain 3 of HCV helicase is stacked with one of the bases of the nucleic acid and is required for its RNA helicase activity, and ATP binding and hydrolysis are suggested to cause rotation of domain 2 relative to domains 1 and 3, which leads to translocation of the protein by one or two bases as the protein ratchets like an inchworm along the strand below domains 1 and 2 (Kim et al., 1998; Kim et al., 2003). In contrast to HCV helicase, flavivirus helicases have no conserved aromatic residue at either end of the presumed single-stranded RNA-binding cleft. In DEN helicase, the pocket next to Ile^{365} could act as a 'helix opener' by disrupting hydrogen bonds at the fork, and the basic concave face between domains II and III would act as a 'translocator' by binding dsRNA ahead of the fork (Sampath et al., 2006). Helicases catalyze various functions such as unwinding the strands of double-helical DNA, removing secondary structures in RNA, and displacing proteins bound to nucleic acid by moving along the nucleic acid unidirectionally either in the 5′ to 3′ or the 3′ to 5′ direction. HCV helicase binds to a substrate with a five-base ssDNA tail at the 3′ end 50 times tighter than a similar substrate with a five-base tail at the 5′ end and unwinds substrates in the 3′ to 5′ direction (Levin et al., 2005). Therefore, JEV helicase structurally similar to HCV helicase may translocate dsRNA in the 3′ to 5′ direction.

In JEV helicase, residues interacting with the phosphodiester backbone may include Arg^{226} (motif Ia), Lys^{367} (motif IV), Arg^{388}, Lys^{389}, Arg^{539} and Arg^{609}. These residues are well conserved in helicases of DEN and YFV, suggesting that residues that participate in the RNA unwinding of flavivirus helicase are different from HCV helicases.

Although the motifs in the active sites of the RNA helicases are well conserved among flaviviruses, HCV, WNV and JEV helicases exhibited a divergent sensitivity to the inhibitors (Borowski et al., 2003), suggesting that these differences are obtained during the evolutional adaptation of each virus to their hosts. Very recently, a single amino acid substitution of Pro for Thr^{249} in the NS3 helicase in a WNV strain with low virulence was shown to be sufficient to generate a virus highly virulent to the American crow (Brault et al., 2007). These results further support the importance of viral helicase for the adaptation of RNA viruses to the changing environment. Many RNA helicases remain to be investigated and further structural analyses of the RNA helicases will provide clues for the development of broad-spectrum or specific antiviral drugs for the treatment of flavivirus infection.

Materials and methods

Expression and purification of JEV NS3 helicase/NTPase

A cDNA encoding the JEV helicase/NTPase domain (amino acid residues 171 to 619 of the AT31 strain) was amplified by polymerase chain reaction (PCR) with the synthetic DNA primers, 5′-AAGAATTCAGCGCCATCGTGCAGGGTGA-3′ and 5′-AACTCGAGTCTCTTTCCTGCTGC-3′. A 1.4 kb region of the PCR-amplified DNA fragment was digested with EcoRI and XhoI, and cloned into the corresponding cloning sites of the *E. coli* expression vector, pET21b (Novagen, San Diego, CA). The expression product is composed of 449 amino acid residues of JEV NS3 helicase/NTPase with the vector-derived 14 amino acid residues at the N-terminus and 6 amino acid residues containing a His-tag (histidine hexamaer) at the C-terminus. The His-tagged JEV helicase/NTPase was expressed in the *E. coli* BL21 (DE3) pLysS strain in the presence of 1 mM isopropyl β-thiogalactoside for 5 h at 20 °C and the bacteria were sonicated in a buffer [20 mM Tris–HCl (pH 8.0) and 500 mM NaCl] with 40 mM imidazole. After centrifugation, the supernatant was applied to a NiTrap HP column (GE Healthcare, Tokyo, Japan) and the resulting nickel-binding proteins were eluted under a linear gradient of 40–400 mM imidazole in the same buffer. After passage through a gel filtration column (HiLoad 16/60 Superdex 200 pg; GE Healthcare), the recombinant protein was applied to an anion exchange column (HiTrap Q; GE Healthcare) and eluted under a linear gradient of 100–400 mM NaCl in 20 mM Tris–HCl buffer (pH 8.0). The final product consists of 469 amino acid residues containing the JEV NS3 NTPase/helicase domain flanked by 14 and 6 amino acid residues at the N-and C-terminus, respectively. Substitution of Ala for the JEV helicase at amino acid residues Gly^{199}, Lys^{200}, Thr^{201}, Gln^{457}, Arg^{458}, Arg^{459}, Gly^{460}, Arg^{461}, Val^{462}, Gly^{463} and Arg^{464}, and mutation at residue Lys^{200} to

Please cite this article as: Yamashita, T., et al., Crystal structure of the catalytic domain of Japanese encephalitis virus NS3 helicase/nucleoside triphosphatase at a resolution of 1.8 Å, Virology (2008), doi:10.1016/j.virol.2007.12.018

Arg, Gln, Asn, Asp, Glu, and His, respectively, were accomplished by PCR-based mutagenesis.

ATPase assay

The colorimetric NTPase assay was conducted by measuring the amount of free phosphate moiety released from nucleoside triphosphate as described previously with minor modifications (Xu et al., 2005). Briefly, 50 μl per well of a reaction mixture containing 10 mM MOPS buffer (pH 6.5), 2 mM NTP, 1 mM $MgCl_2$ and 0.1 μg of purified JEV NS3 NTPase/helicase protein was incubated in a 96-well plate at room temperature for 30 min, and 100 μl of dye solution (water: 0.081% malachite green in water: 5.7% ammonium molybdate in 6 N HCl: 2.3% polyvinylalchol in water=2:2:1:1, v/v) was added. Color development was terminated by addition of 25 μl of 30% sodium citrate after 5 min of incubation, and the absorbance at 620 nm was determined.

RNA helicase assay

The labeled single-stranded RNA fragment was synthesized by Riboprobe Systems (Promega, Madison, WI) using a pSP72 DNA fragment linearized with BamHI as a template in the presence of [α-^{32}P]UTP (3000 Ci/mmol; GE Healthcare). Plasmid pGEM-3Zf(+) (Promega) was linearized with EaeI and non-labeled RNA fragment was prepared. The RNA transcripts were resuspended in 100 μl of annealing buffer [10 mM Tris–HCl (pH 8.5), 100 mM NaCl, 8 fmol of each transcript], boiled for 5 min and hybridized at room temperature overnight. Schematic representation of the double-stranded RNA substrate is shown in Fig. 5D. The RNA helicase assay was carried out in 20 μl of helicase buffer containing 25 mM MES (pH 6.0), 2 mM DTT, 2 mM $MgCl_2$, 5 mM ATP, 1.25 U of RNase inhibitor (Promega), 0.32 fmol of the RNA substrate and 0.1 μg of purified JEV NS3 NTPase/helicase protein at 37 °C for 30 min. The reaction was terminated with 5 μl of loading buffer [100 mM Tris–HCl (pH 7.4), 5 mM EDTA, 0.5% SDS, 50% glycerol, 0.1% xylene cyanol, 0.1% bromophenol blue] and analyzed by 10% native polyacrylamide gel electrophoresis (PAGE). The autoradiographic pattern was obtained by using a BAS 1500 Image Analyzing System (Fujifilm, Tokyo, Japan).

Crystallization of JEV NS3 helicase/NTPase

Crystallization of the JEV NS3 helicase/NTPase domain was carried out under conditions screened by the hanging-drop vapor-diffusion method by Wizard I and II kits (Emerald BioSystems, Bainbridge Island, WA). The purified protein solution (2 μl) at a concentration of 10 mg/ml in a buffer [20 mM Tris–HCl (pH 8.0) and 250 mM NaCl] was equilibrated with 0.4 ml of a reservoir solution containing 15% ethanol and 100 mM Tris–HCl (pH 7.0) at 25 °C. The size and quality of the crystals were further improved by an addition of 4% pentaerythritol etoxylate (3/4 EO/OH). As a result, single crystals with dimensions of 0.5 × 0.3 × 0.2 mm were obtained in the drop after 5 days of incubation (Fig. 1B).

Data collection and processing

The crystal of the JEV NS3 helicase/NTPase domain was soaked in the reservoir solution with 30% (w/v) glycerol for 1 min and mounted in nylon CryoLoops (Hampton Research, Aliso Viejo, CA). Then, it was placed directly into a nitrogen stream at 100K. Data were collected at a beamline BL44XU of SPring-8 (Hyogo, Japan) using a DIP6040 imaging plate (Mac Science, Yokohama, Japan). The oscillation ranges were 200° with oscillations per frame being 1°. Oscillation data were recorded in frame 1° oscillation with 3-second exposure time for each image. The data were processed using the computer program HKL2000. The statistics of the diffraction data are summarized in Table 1. The space group was determined to be monoclinic $P2_1$. Assuming that there is one molecule of JEV NS3 helicase/NTPase domain in the asymmetric unit, the value of the Matthews content V_M (Matthews, 1968) is 2.2 Å^3 Da^{-1}, corresponding to a solvent content of 48%, both of which are within the normal range of values for protein crystals (Matthews, 1968).

Phasing model building, structure refinement, and analysis

The structure model was determined by the molecular replacement method using Molrep (Vagin and Teplyakov, 2000). The DEN helicase/NTPase domain (Protein Data Bank entry 2BHR) (Xu et al., 2005) was used as an initial search model. All refinement were carried out using REFMAC (Murshudov et al., 1997). About 50% of the model was autobuilt into the 1.8 Å electron density using wARP (Perrakis et al., 1997). An essential complete model was built into this map with program O (Jones et al., 1991). The refined model consisted of JEV helicase/NTPase domain in an asymmetric unit. The final coordinates and structure factor have been submitted to the Protein Data Bank with accession number 2Z83. In a final model, four regions, amino acid residues 171 to 180, 245 to 254, 274 to 276 and 412 to 416, are disordered and not included. No residues are in the disallowed region of the Ramachandoran plot. The final statistics are summarized in Table 1. Figs. 1C, 2, 3, and 5A were drawn by using the program PyMol and Fig. 4 was drawn using Molscript (Esnouf, 1999) and Raster 3D (Merritt and Murphy, 1994). The superposition of the structure and calculation of the root mean square (RMS) deviation were carried out using the program LASQKAB from the CCP4 suite (Collaborative Computational Project Number 4, 1994). We calculated the electrostatic potentials of the JEV helicase/NTPase domain by GRASP program (Nicholls et al., 1991).

Hypothetical ATP-binding model

An ATP-binding model of the JEV helicase domain was built with O (Jones et al., 1991) The structural data of the ATP molecule was obtained from a PDB file, 1xdn.

Generation of JEV from plasmid

As described above, mutations in the JEV helicase were introduced in the plasmid pMWJEATG1 carrying a full-length

Please cite this article as: Yamashita, T., et al., Crystal structure of the catalytic domain of Japanese encephalitis virus NS3 helicase/nucleoside triphosphatase at a resolution of 1.8 Å, Virology (2008), doi:10.1016/j.virol.2007.12.018

cDNA of the JEV AT31 strain under the control of a T7 promoter (Zhao et al., 2005) by PCR-based mutagenesis. The plasmid DNAs encoding the wild type or mutant JEVs digested with KpnI were used as templates for RNA synthesis. Capped, full-length JEV RNAs were synthesized *in vitro* by an mMESSAGE mMACHINE T7 kit (Ambion, Austin, TX), purified by precipitation with lithium chloride, and used for electroporation into Vero (African green monkey kidney) cells maintained in Dulbecco's modified Eagle's minimal essential medium supplemented with 10% fetal bovine serum as described previously (Mori et al., 2005).

Acknowledgments

We thank H. Murase for her secretarial work. We also thank the staff of SPring-8 BL44XU beamline for their assistance with the data collection. This work was supported in part by grants-in-aid from the Ministry of Health, Labor and Welfare; the 21st Century Center of Excellence Program of Japan; the Ministry of Education, Culture, Sports, Science and Technology of Japan; the Foundation for Research Collaboration Center on Emerging and Re-emerging Infections; and the Zoonoses Control Project of the Ministry of Agriculture, Forestry and Fisheries of Japan.

References

Ahmadian, M.R., Stege, P., Scheffzek, K., Wittinghofer, A., 1997. Confirmation of the arginine-finger hypothesis for the GAP-stimulated GTP-hydrolysis reaction of Ras. Nat. Struct. Biol. 4, 686–689.

Borowski, P., Deinert, J., Schalinski, S., Bretner, M., Ginalski, K., Kulikowski, T., Shugar, D., 2003. Halogenated benzimidazoles and benzotriazoles as inhibitors of the NTPase/helicase activities of hepatitis C and related viruses. Eur. J. Biochem. 270, 1645–1653.

Brault, A.C., Huang, C.Y., Langevin, S.A., Kinney, R.M., Bowen, R.A., Ramey, W.N., Panella, N.A., Holmes, E.C., Powers, A.M., Miller, B.R., 2007. A single positively selected West Nile viral mutation confers increased virogenesis in American crows. Nat. Genet. 39, 1162–1166.

Caruthers, J.M., McKay, D.B., 2002. Helicase structure and mechanism. Curr. Opin. Struct. Biol. 12, 123–133.

Cho, H.S., Ha, N.C., Kang, L.W., Chung, K.M., Back, S.H., Jang, S.K., Oh, B.H., 1998. Crystal structure of RNA helicase from genotype 1b hepatitis C virus. A feasible mechanism of unwinding duplex RNA. J. Biol. Chem. 273, 15045–15052.

Collaborative Computational Project Number 4, 1994. The CCP4 suite: programs for protein crystallography. Acta Crystallogr. D. Biol. Crystallogr. 50, 760–763.

Cui, T., Sugrue, R.J., Xu, Q., Lee, A.K., Chan, Y.C., Fu, J., 1998. Recombinant dengue virus type 1 NS3 protein exhibits specific viral RNA binding and NTPase activity regulated by the NS5 protein. Virology 246, 409–417.

Esnouf, R.M., 1999. Further additions to MolScript version 1.4, including reading and contouring of electron-density maps. Acta Crystallogr. D. Biol. Crystallogr. 55, 938–940.

Jones, T.A., Zou, J.Y., Cowan, S.W., Kjeldgaard, 1991. Improved methods for building protein models in electron density maps and the location of errors in these models. Acta Crystallogr. A. 47, 110–119.

Kim, D.W., Kim, J., Gwack, Y., Han, J.H., Choe, J., 1997. Mutational analysis of the hepatitis C virus RNA helicase. J. Virol. 71, 9400–9409.

Kim, J.L., Morgenstern, K.A., Griffith, J.P., Dwyer, M.D., Thomson, J.A., Murcko, M.A., Lin, C., Caron, P.R., 1998. Hepatitis C virus NS3 RNA helicase domain with a bound oligonucleotide: the crystal structure provides insights into the mode of unwinding. Structure 6, 89–100.

Kim, J.W., Seo, M.Y., Shelat, A., Kim, C.S., Kwon, T.W., Lu, H.H., Moustakas, D.T., Sun, J., Han, J.H., 2003. Structurally conserved amino Acid w501 is required for RNA helicase activity but is not essential for DNA helicase activity of hepatitis C virus NS3 protein. J. Virol. 77, 571–582.

Koonin, E.V., 1991. Similarities in RNA helicases. Nature 352, 290.

Korolev, S., Hsieh, J., Gauss, G.H., Lohman, T.M., Waksman, G., 1997. Major domain swiveling revealed by the crystal structures of complexes of *E. coli* Rep helicase bound to single-stranded DNA and ADP. Cell 90, 635–647.

Kuo, M.D., Chin, C., Hsu, S.L., Shiao, J.Y., Wang, T.M., Lin, J.H., 1996. Characterization of the NTPase activity of Japanese encephalitis virus NS3 protein. J. Gen. Virol. 77, 2077–2084.

Kwong, A.D., Rao, B.G., Jeang, K.T., 2005. Viral and cellular RNA helicases as antiviral targets. Nat. Rev. Drug Discov. 4, 845–853.

Levin, M.K., Gurjar, M., Patel, S.S., 2005. A Brownian motor mechanism of translocation and strand separation by hepatitis C virus helicase. Nat. Struct. Mol. Biol. 12, 429–435.

Li, H., Clum, S., You, S., Ebner, K.E., Padmanabhan, R., 1999a. The serine protease and RNA-stimulated nucleoside triphosphatase and RNA helicase functional domains of dengue virus type 2 NS3 converge within a region of 20 amino acids. J. Virol. 73, 3108–3116.

Li, J., Tang, H., Mullen, T.M., Westberg, C., Reddy, T.R., Rose, D.W., Wong-Staal, F., 1999b. A role for RNA helicase A in post-transcriptional regulation of HIV type 1. Proc. Natl. Acad. Sci. U. S. A. 96, 709–714.

Luking, A., Stahl, U., Schmidt, U., 1998. The protein family of RNA helicases. Crit. Rev. Biochem. Mol. Biol. 33, 259–296.

Marians, K.J., 1997. Helicase structures: a new twist on DNA unwinding. Structure 5, 1129–1134.

Matthews, B.W., 1968. Solvent content of protein crystals. J. Mol. Biol. 33, 491–497.

Matusan, A.E., Kelley, P.G., Pryor, M.J., Whisstock, J.C., Davidson, A.D., Wright, P.J., 2001. Mutagenesis of the dengue virus type 2 NS3 proteinase and the production of growth-restricted virus. J. Gen. Virol. 82, 1647–1656.

Merritt, E.A., Murphy, M.E., 1994. Raster3D Version 2.0. A program for photorealistic molecular graphics. Acta Crystallogr. D. Biol. Crystallogr. 50, 869–873.

Mori, Y., Okabayashi, T., Yamashita, T., Zhao, Z., Wakita, T., Yasui, K., Hasebe, F., Tadano, M., Konishi, E., Moriishi, K., Matsuura, Y., 2005. Nuclear localization of Japanese encephalitis virus core protein enhances viral replication. J. Virol. 79, 3448–3458.

Murshudov, G.N., Vagin, A.A., Dodson, E.J., 1997. Refinement of macromolecular structures by the maximum-likelihood method. Acta Crystallogr. D. Biol. Crystallogr. 53, 240–255.

Nakagawa, N., Masui, R., Kato, R., Kuramitsu, S., 1997. Domain structure of *Thermus thermophilus* UvrB protein. Similarity in domain structure to a helicase. J. Biol. Chem. 272, 22703–22713.

Nicholls, A., Sharp, K.A., Honig, B., 1991. Protein folding and association: insights from the interfacial and thermodynamic properties of hydrocarbons. Proteins 11, 281–296.

Niedenzu, T., Roleke, D., Bains, G., Scherzinger, E., Saenger, W., 2001. Crystal structure of the hexameric replicative helicase RepA of plasmid RSF1010. J. Mol. Biol. 306, 479–487.

Perrakis, A., Sixma, T.K., Wilson, K.S., Lamzin, V.S., 1997. wARP: improvement and extension of crystallographic phases by weighted averaging of multiple-refined dummy atomic models. Acta Crystallogr. D. Biol. Crystallogr. 53, 448–455.

Sampath, A., Xu, T., Chao, A., Luo, D., Lescar, J., Vasudevan, S.G., 2006. Structure-based mutational analysis of the NS3 helicase from dengue virus. J. Virol. 80, 6686–6690.

Schmid, S.R., Linder, P., 1992. D-E-A-D protein family of putative RNA helicases. Mol. Microbiol. 6, 283–291.

Sengoku, T., Nureki, O., Nakamura, A., Kobayashi, S., Yokoyama, S., 2006. Structural basis for RNA unwinding by the DEAD-box protein *Drosophila* Vasa. Cell 125, 287–300.

Solomon, T., Ni, H., Beasley, D.W., Ekkelenkamp, M., Cardosa, M.J., Barrett, A.D., 2003. Origin and evolution of Japanese encephalitis virus in southeast Asia. J. Virol. 77, 3091–3098.

Subramanya, H.S., Bird, L.E., Brannigan, J.A., Wigley, D.B., 1996. Crystal structure of a DExx box DNA helicase. Nature 384, 379–383.

Please cite this article as: Yamashita, T., et al., Crystal structure of the catalytic domain of Japanese encephalitis virus NS3 helicase/nucleoside triphosphatase at a resolution of 1.8 Å, Virology (2008), doi:10.1016/j.virol.2007.12.018

Sumiyoshi, H., Mori, C., Fuke, I., Morita, K., Kuhara, S., Kondou, J., Kikuchi, Y., Nagamatu, H., Igarashi, A., 1987. Complete nucleotide sequence of the Japanese encephalitis virus genome RNA. Virology 161, 497–510.

Tanner, N.K., Cordin, O., Banroques, J., Doere, M., Linder, P., 2003. The Q motif: a newly identified motif in DEAD box helicases may regulate ATP binding and hydrolysis. Mol. Cell 11, 127–138.

Theis, K., Chen, P.J., Skorvaga, M., Van Houten, B., Kisker, C., 1999. Crystal structure of UvrB, a DNA helicase adapted for nucleotide excision repair. Embo J. 18, 6899–6907.

Tsai, T.F., 2000. New initiatives for the control of Japanese encephalitis by vaccination: minutes of a WHO/CVI meeting, Bangkok, Thailand, 13–15 October 1998. Vaccine 18 (Suppl 2), 1–25.

Utama, A., Shimizu, H., Hasebe, F., Morita, K., Igarashi, A., Shoji, I., Matsuura, Y., Hatsu, M., Takamizawa, K., Hagiwara, A., Miyamura, T., 2000a. Role of the DExH motif of the Japanese encephalitis virus and hepatitis C virus NS3 proteins in the ATPase and RNA helicase activities. Virology 273, 316–324.

Utama, A., Shimizu, H., Morikawa, S., Hasebe, F., Morita, K., Igarashi, A., Hatsu, M., Takamizawa, K., Miyamura, T., 2000b. Identification and characterization of the RNA helicase activity of Japanese encephalitis virus NS3 protein. FEBS Lett. 465, 74–78.

Vagin, A., Teplyakov, A., 2000. An approach to multi-copy search in molecular replacement. Acta Crystallogr. D. Biol. Crystallogr. 56, 1622–1624.

Velankar, S.S., Soultanas, P., Dillingham, M.S., Subramanya, H.S., Wigley, D.B., 1999. Crystal structures of complexes of PcrA DNA helicase with a DNA substrate indicate an inchworm mechanism. Cell 97, 75–84.

Warrener, P., Tamura, J.K., Collett, M.S., 1993. RNA-stimulated NTPase activity associated with yellow fever virus NS3 protein expressed in bacteria. J. Virol. 67, 989–996.

Wengler, G., Wengler, G., 1991. The carboxy-terminal part of the NS 3 protein of the West Nile flavivirus can be isolated as a soluble protein after proteolytic cleavage and represents an RNA-stimulated NTPase. Virology 184, 707–715.

Wu, J., Bera, A.K., Kuhn, R.J., Smith, J.L., 2005. Structure of the flavivirus helicase: implications for catalytic activity, protein interactions, and proteolytic processing. J. Virol. 79, 10268–10277.

Xu, T., Sampath, A., Chao, A., Wen, D., Nanao, M., Chene, P., Vasudevan, S.G., Lescar, J., 2005. Structure of the Dengue virus helicase/nucleoside triphosphatase catalytic domain at a resolution of 2.4 A. J. Virol. 79, 10278–10288.

Yao, N., Hesson, T., Cable, M., Hong, Z., Kwong, A.D., Le, H.V., Weber, P.C., 1997. Structure of the hepatitis C virus RNA helicase domain. Nat. Struct. Biol. 4, 463–467.

Yao, N., Reichert, P., Taremi, S.S., Prosise, W.W., Weber, P.C., 1999. Molecular views of viral polyprotein processing revealed by the crystal structure of the hepatitis C virus bifunctional protease-helicase. Structure 7, 1353–1363.

Zhao, Z., Date, T., Li, Y., Kato, T., Miyamoto, M., Yasui, K., Wakita, T., 2005. Characterization of the E-138 (Glu/Lys) mutation in Japanese encephalitis virus by using a stable, full-length, infectious cDNA clone. J. Gen. Virol. 86, 2209–2220.

Please cite this article as: Yamashita, T., et al., Crystal structure of the catalytic domain of Japanese encephalitis virus NS3 helicase/nucleoside triphosphatase at a resolution of 1.8 Å, Virology (2008), doi:10.1016/j.virol.2007.12.018

Critical role of PA28γ in hepatitis C virus-associated steatogenesis and hepatocarcinogenesis

Kohji Moriishi*, Rika Mochizuki*, Kyoji Moriya†, Hironobu Miyamoto*, Yoshio Mori*, Takayuki Abe*, Shigeo Murata‡, Keiji Tanaka‡, Tatsuo Miyamura§, Tetsuro Suzuki§, Kazuhiko Koike†, and Yoshiharu Matsuura*¶

*Department of Molecular Virology, Research Institute for Microbial Diseases, Osaka University, Osaka 565-0871, Japan; †Department of Internal Medicine, Graduate School of Medicine, University of Tokyo, Tokyo 113-8655, Japan; ‡Department of Molecular Oncology, Tokyo Metropolitan Institute of Medical Science, Tokyo 113-8613, Japan; and §Department of Virology II, National Institute of Infectious Diseases, Tokyo 162-8640, Japan

Edited by Peter Palese, Mount Sinai School of Medicine, New York, NY, and approved December 1, 2006 (received for review August 23, 2006)

Hepatitis C virus (HCV) is a major cause of chronic liver disease that frequently leads to steatosis, cirrhosis, and eventually hepatocellular carcinoma (HCC). HCV core protein is not only a component of viral particles but also a multifunctional protein because liver steatosis and HCC are developed in HCV core gene-transgenic (CoreTg) mice. Proteasome activator PA28γ/REGγ regulates host and viral proteins such as nuclear hormone receptors and HCV core protein. Here we show that a knockout of the PA28γ gene induces the accumulation of HCV core protein in the nucleus of hepatocytes of CoreTg mice and disrupts development of both hepatic steatosis and HCC. Furthermore, the genes related to fatty acid biosynthesis and *srebp-1c* promoter activity were up-regulated by HCV core protein in the cell line and the mouse liver in a PA28γ-dependent manner. Heterodimer composed of liver X receptor α (LXRα) and retinoid X receptor α (RXRα) is known to up-regulate *srebp-1c* promoter activity. Our data also show that HCV core protein enhances the binding of LXRα/RXRα to LXR-response element in the presence but not the absence of PA28γ. These findings suggest that PA28γ plays a crucial role in the development of liver pathology induced by HCV infection.

fatty acid | proteasome | sterol regulatory element-binding protein (SREBP) | RXRα | LXRα

Hepatitis C virus (HCV) belongs to the Flaviviridae family, and it possesses a positive, single-stranded RNA genome that encodes a single polyprotein composed of ≈3,000 aa. The HCV polyprotein is processed by host and viral proteases, resulting in 10 viral proteins. Viral structural proteins, including the capsid (core) protein and two envelope proteins, are located in the N-terminal one-third of the polyprotein, followed by nonstructural proteins.

HCV infects >170 million individuals worldwide, and then it causes liver disease, including hepatic steatosis, cirrhosis, and eventually hepatocellular carcinoma (HCC) (1). The prevalence of fatty infiltration in the livers of chronic hepatitis C patients has been reported to average ≈50% (2, 3), which is higher than the percentage in patients infected with hepatitis B virus and other liver diseases. However, the precise functions of HCV proteins in the development of fatty liver remain unknown because of the lack of a system sufficient to investigate the pathogenesis of HCV. HCV core protein expression has been shown to induce lipid droplets in cell lines and hepatic steatosis and HCC in transgenic mice (4–6). These reports suggest that HCV core protein plays an important role in the development of various types of liver failure, including steatosis and HCC.

Recent reports suggest that lipid biosynthesis affects HCV replication (7–9). Involvement of a geranylgeranylated host protein, FBL2, in HCV replication through the interaction with NS5A suggests that the cholesterol biosynthesis pathway is also important for HCV replication (9). Increases in saturated and monounsaturated fatty acids enhance HCV RNA replication, whereas increases in polyunsaturated fatty acids suppress it (7). Lipid homeostasis is regulated by a family of steroid regulatory element-binding proteins (SREBPs), which activate the expression of >30 genes involved in the synthesis and uptake of cholesterol, fatty acids, triglycerides, and phospholipids. Biosynthesis of cholesterol is regulated by SREBP-2, whereas that of fatty acids, triglycerides, and phospholipids is regulated by SREBP-1c (10–14). In chimpanzees, host genes involved in SREBP signaling are induced during the early stages of HCV infection (8). SREBP-1c regulates the transcription of acetyl-CoA carboxylase, fatty acid synthase, and stearoyl-CoA desaturase, leading to the production of saturated and monounsaturated fatty acids and triglycerides (15). SREBP-1c is transcriptionally regulated by liver X receptor (LXR) α and retinoid X receptor (RXR) α, which belong to a family of nuclear hormone receptors (15, 16). Accumulation of cellular fatty acids by HCV core protein is expected to be modulated by the SREBP-1c pathway because RXRα is activated by HCV core protein (17). However, it remains unknown whether HCV core protein regulates the *srebp-1c* promoter.

We previously reported (18) that HCV core protein specifically binds to the proteasome activator PA28γ/REGγ in the nucleus and is degraded through a PA28γ-dependent pathway. PA28γ is well conserved from invertebrates to vertebrates, and amino acid sequences of human and murine PA28γs are identical (19). The homologous proteins, PA28α and PA28β, form a heteroheptamer in the cytoplasm, and they activate chymotrypsin-like peptidase activity of the 20S proteasome, whereas PA28γ forms a homoheptamer in the nucleus, and it enhances trypsin-like peptidase activity of 20S proteasome (20). Recently, Li and colleagues (21) reported that PA28γ binds to steroid receptor coactivator-3 (SRC-3) and enhances the degradation of SRC-3 in a ubiquitin- and ATP-independent manner. However, the precise physiological functions of PA28γ are largely unknown *in vivo*. In this work, we examine whether PA28γ is required for liver pathology induced by HCV core protein *in vivo*.

Results

PA28γ-Knockout HCV Core Gene Transgenic Mice. To determine the role of PA28γ in HCV core-induced steatosis and the development of HCC *in vivo*, we prepared PA28γ-knockout core gene transgenic mice. The PA28γ-deficient, PA28γ$^{-/-}$ mice were born without

Author contributions: K. Moriishi, K.T., T.M., T.S., K.K., and Y. Matsuura designed research; K. Moriishi, R.M., K. Moriya, H.M., Y. Mori, and T.A. performed research; S.M. contributed new reagents/analytic tools; Y. Matsuura analyzed data; and K. Moriishi, K.K., and Y. Matsuura wrote the paper.

The authors declare no conflict of interest.

This article is a PNAS direct submission.

Freely available online through the PNAS open access option.

Abbreviations: CoreTg, HCV core gene-transgenic; HCC, hepatocellular carcinoma; HCV, hepatitis C virus; LXR, liver X receptor; LXRE, liver X receptor-response element; MEF, mouse embryonic fibroblast; ROS, reactive oxygen species; RXR, retinoid X receptor; SRC-3, steroid receptor coactivator-3; SREBP, steroid regulatory element-binding protein.

¶To whom correspondence should be addressed. E-mail: matsuura@biken.osaka-u.ac.jp.

This article contains supporting information online at www.pnas.org/cgi/content/full/0607312104/DC1.

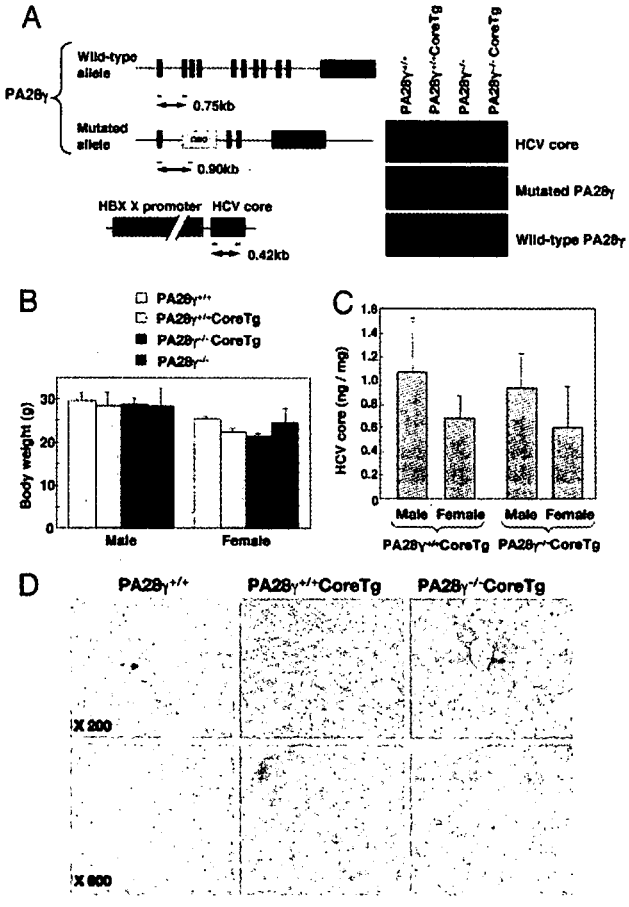

Fig. 1. Preparation and characterization of PA28γ-knockout HCV core-transgenic mice. (*A*) The structures of the wild-type and mutated PA28γ genes and the transgene encoding the HCV core protein under the control of the HBV X promoter were investigated. Positions corresponding to the screening primers and sizes of PCR products are shown. PCR products of the HCV core gene as well as wild-type and mutated PA28γ alleles were amplified from the genomic DNAs of PA28γ$^{+/+}$, PA28γ$^{+/+}$CoreTg, PA28γ$^{-/-}$, and PA28γ$^{-/-}$CoreTg mice. (*B*) Body weights of PA28γ$^{+/+}$, PA28γ$^{+/+}$CoreTg, PA28γ$^{-/-}$CoreTg, and PA28γ$^{-/-}$ mice at the age of 6 months. (*C*) HCV core protein levels in the livers of PA28γ$^{+/+}$CoreTg and PA28γ$^{-/-}$CoreTg mice were determined by ELISA (mean ± SD, $n = 10$). (*D*) Localization of HCV core protein in the liver. Liver sections of PA28γ$^{+/+}$, PA28γ$^{+/+}$CoreTg, and PA28γ$^{-/-}$CoreTg mice at the age of 2 months were stained with anti-HCV core antibody.

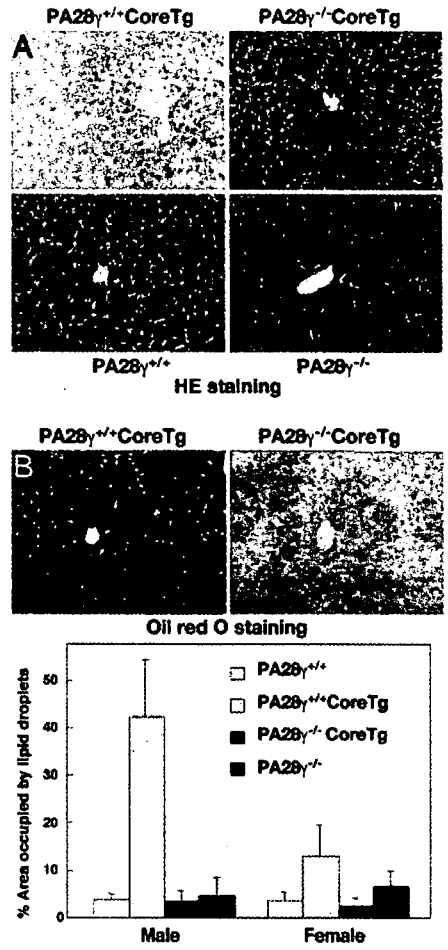

Fig. 2. Accumulation of lipid droplets by expression of HCV core protein. (*A*) Liver sections of the mice at the age of 6 months were stained with hematoxylin/eosin (HE). (*B*) (*Upper*) Liver sections of PA28γ$^{+/+}$CoreTg and PA28γ$^{-/-}$CoreTg mice at the age of 6 months were stained with oil red O. (*Lower*) The area occupied by lipid droplets of PA28γ$^{+/+}$ (white), PA28γ$^{+/+}$CoreTg (gray), PA28γ$^{-/-}$CoreTg (black), and PA28γ$^{-/-}$ (dark gray) mice was calculated by Image-Pro software (MediaCybernetics, Silver Spring, MD) (mean ± SD, $n = 10$).

appreciable abnormalities in all tissues examined, with the exception of a slight retardation of growth (22). HCV core gene-transgenic (PA28γ$^{+/+}$CoreTg) mice were bred with PA28γ$^{-/-}$ mice to create PA28γ$^{+/-}$CoreTg mice. The PA28γ$^{+/-}$CoreTg offspring were bred with each other, and PA28γ$^{-/-}$CoreTg mice were selected by PCR using primers specific to the target sequences (Fig. 1*A*). No significant differences in body weight were observed among the 6-month-old mice, although PA28γ$^{-/-}$ mice exhibited a slight retardation of growth (Fig. 1*B*). A similar level of PA28γ expression was detected in PA28γ$^{+/+}$CoreTg and PA28γ$^{+/+}$ mice (see Fig. 5*B*). The expression levels and molecular size of HCV core protein were similar in the livers of PA28γ$^{+/+}$CoreTg and PA28γ$^{-/-}$CoreTg mice (Fig. 1*C*; see also Fig. 5*B*).

PA28γ Is Required for Degradation of HCV Core Protein in the Nucleus and Induction of Liver Steatosis. HCV core protein has been detected at various sites, such as the endoplasmic reticulum, mitochondria, lipid droplets, and nucleus of cultured cell lines, as well as in hepatocytes of PA28γ$^{+/+}$CoreTg mice and hepatitis C patients (6, 23, 24). Although HCV core protein is predominantly detected in the cytoplasm of the liver cells of PA28γ$^{+/+}$CoreTg mice, as reported in ref. 6, in the present study a clear accumulation of HCV core protein was observed in the liver cell nuclei of PA28γ$^{-/-}$CoreTg mice (Fig. 1*D*). These findings clearly indicate that at least some fraction of the HCV core protein is translocated into the nucleus and is degraded through a PA28γ-dependent pathway. Mild vacuolation was observed in the cytoplasm of the liver cells of 4-month-old PA28γ$^{+/+}$CoreTg mice, and it became more severe at 6 months, as reported in ref. 25. Hematoxylin/eosin-stained liver sections of 6-month-old PA28γ$^{+/+}$CoreTg mice exhibited severe vacuolating lesions (Fig. 2*A*), which were clearly stained with oil red O (Fig. 2*B Upper*), whereas no such lesions were detected in the livers of PA28γ$^{-/-}$CoreTg, PA28γ$^{+/+}$, or PA28γ$^{-/-}$ mice at the same age. The areas occupied by the lipid droplets in the PA28γ$^{+/+}$CoreTg mouse livers were ≈10 and 2–4 times larger than those of male and female of PA28γ$^{+/+}$, PA28γ$^{-/-}$, and PA28γ$^{-/-}$CoreTg mice, respectively (Fig. 2*B Lower*). These results suggest that PA28γ is required for the induction of liver steatosis by HCV core protein in mice.

PA28γ Is Required for the Up-Regulation of SREBP-1c Transcription by HCV Core Protein in the Mouse Liver. To clarify the effects of a knockout of the PA28γ gene in PA28γ$^{+/+}$CoreTg mice on lipid

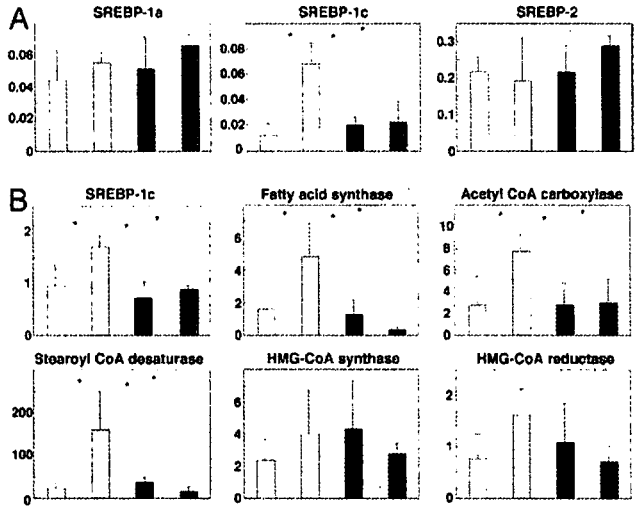

Fig. 3. Transcription of genes regulating lipid biosynthesis in the mouse liver. (*A*) Total RNA was prepared from the livers of 2-month-old mice; and the transcription of genes encoding SREBP-1a, SREBP-1c, and SREBP-2 was determined by real-time PCR. (*B*) The transcription of genes encoding SREBP-1c, fatty acid synthase, acetyl-CoA carboxylase, stearoyl-CoA desaturase, HMG-CoA synthase, and HMG-CoA reductase of 6-month-old mice was measured by real-time PCR. The transcription of the genes was normalized with that of hypoxanthine phosphoribosyltransferase, and the values are expressed as relative activity ($n = 5$; *, $P < 0.05$; **, $P < 0.01$). The transcription of each gene in PA28$\gamma^{+/+}$, PA28$\gamma^{+/+}$CoreTg, PA28$\gamma^{-/-}$CoreTg, and PA28$\gamma^{-/-}$ mice is indicated by white, gray, black, and dark gray bars, respectively.

metabolism, genes related to the lipid biosyntheses were examined by real-time quantitative PCR. Transcription of SREBP-1c was higher in the livers of PA28$\gamma^{+/+}$CoreTg mice than in those of PA28$\gamma^{+/+}$, PA28$\gamma^{-/-}$, and PA28$\gamma^{-/-}$CoreTg mice at 2 months of age, but no such increases in SREBP-2 and SREBP-1a were observed (Fig. 3*A*). Although transcription of SREBP-1c and its regulating enzymes, such as acetyl-CoA carboxylase, fatty acid synthase, and stearoyl-CoA desaturase, was also enhanced in the livers of 6-month-old PA28$\gamma^{+/+}$CoreTg mice compared with the levels in the livers of PA28$\gamma^{+/+}$, PA28$\gamma^{-/-}$, and PA28$\gamma^{-/-}$CoreTg mice, no statistically significant differences were observed with respect to the transcription levels of cholesterol biosynthesis-related genes that are regulated by SREBP-2 (e.g., HMG-CoA synthase and HMG-CoA reductase) (Fig. 3*B*). These results suggest the following: (*i*) the up-regulation of SREBP-1c transcription in the livers of mice requires both HCV core protein and PA28γ, and (*ii*) the nuclear accumulation of HCV core protein alone, which occurs because of the lack of degradation along a PA28γ-dependent proteasome pathway, does not activate the *srebp-1c* promoter.

HCV Core Protein Indirectly Potentiates *srebp-1c* Promoter Activity in an LXRα/RXRα-Dependent Manner. LXRα, which is primarily expressed in the liver, forms a complex with RXRα and synergistically potentiates *srebp-1c* promoter activity (16). Activation of RXRα by HCV core protein suggests that cellular fatty acid synthesis is modulated by the SREBP-1c pathway, although HCV core protein was not included in the transcription factor complex in the electrophoresis mobility shift assay (EMSA) (17). To analyze the effect of HCV core protein and PA28γ on the activation of the *srebp-1c* promoter, we first examined the effect of HCV core protein on the binding of the LXRα/RXRα complex to the LXR-response element (LXRE) located upstream of the SREBP-1c gene (Fig. 4*A*). Although a weak shift of the labeled LXRE probe was observed by incubation with nuclear extracts prepared from 293T cells expressing FLAG-tagged LXRα and HA-tagged RXRα, a clear shift was obtained by the treatment of cells with 9-*cis*-retinoic acid and 22(*R*)-hydroxylcholesterol, ligands for LXRα and RXRα, respectively. In contrast, coexpression of HCV core protein with LXRα and RXRα potentiated the shift of the probe irrespective of the treatment with the ligands. Addition of 500 times the amount of nonlabeled LXRE probe (competitor) diminished the shift of the labeled probe induced by the ligands and/or HCV core protein. Furthermore, coincubation of the nuclear fraction with antibody to FLAG or HA tag but not with antibody to either HCV core or PA28γ caused a supershift of the labeled probe. These results indicate that HCV core protein does not participate in the LXRα/RXRα–LXRE complex but indirectly enhances the binding of LXRα/RXRα to the LXRE.

The activity of the *srebp-1c* promoter was enhanced by the expression of HCV core protein in 293T cells, and it was further enhanced by coexpression of LXRα/RXRα (Fig. 4*B*). Enhancement of the *srebp-1c* promoter by coexpression of HCV core protein and LXRα/RXRα was further potentiated by treatment with the ligands for LXRα and RXRα. The cells treated with 9-*cis*-retinoic acid exhibited more potent enhancement of the *srebp-1c* promoter than those treated with 22(*R*)-hydroxylcholesterol. HCV core protein exhibited more potent enhancement of the *srebp-1c* promoter in cells treated with both ligands than in those treated with either ligand alone. These results suggest that HCV core protein poten-

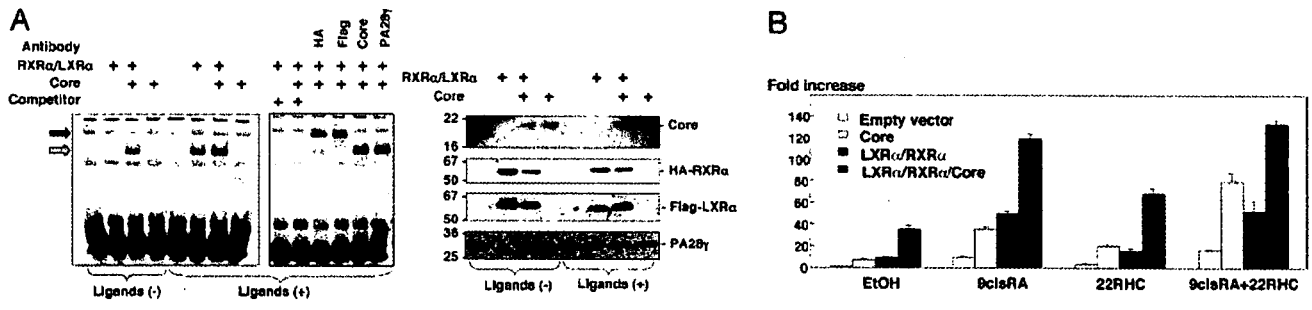

Fig. 4. Activation of the *srebp-1c* promoter by HCV core protein. (*A*) FLAG-LXRα and HA-RXRα were expressed in 293T cells together with or without HCV core protein. Ligands for LXRα and RXRα dissolved in ethanol [Ligands (+)] or ethanol alone [Ligands (−)] were added to the culture supernatant at 24 h posttransfection. Cells were harvested at 48 h posttransfection, and nuclear extracts were mixed with the reaction buffer for EMSA in the presence or absence of antibody (100 ng) against HA, FLAG, HCV core or PA28γ, or nonlabeled LXRE probe (Competitor). (*Left*) The resulting mixtures were subjected to PAGE and blotted with horseradish peroxidase/streptavidin. The mobility shift of the LXRE probe and its supershift are indicated by a gray and black arrow, respectively. (*Right*) Expression of HCV core, HA-RXRα, FLAG-LXRα, and PA28γ in cells was detected by immunoblotting. (*B*) Effects of ligands for RXRα, 9-*cis*-retinoic acid (9cisRA), and for LXRα, 22(*R*)-hydroxylcholesterol (22RHC), on the activation of the *srebp-1c* promoter in 293T cells expressing RXRα, LXRα, and/or HCV core protein. Ligands were added into the medium at 24 h posttransfection at a concentration of 5 μM, and the cells were harvested after 24 h of incubation.

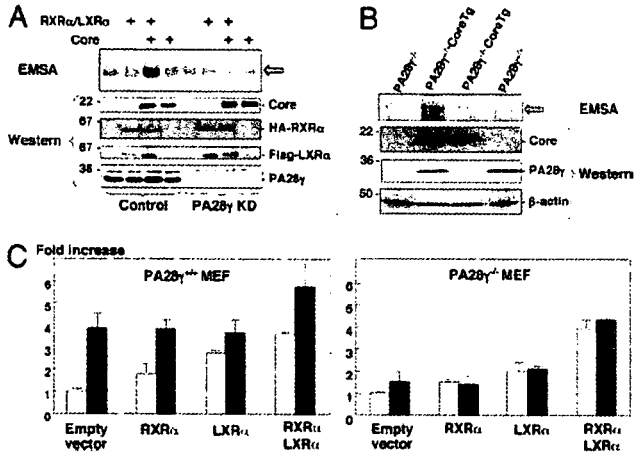

Fig. 5. PA28γ is required for HCV core-dependent activation of the *srebp-1c* promoter. (*A*) Effect of PA28γ knockdown on the LXRα/RXRα–DNA complex. FLAG-LXRα and HA-RXRα were expressed in FLC4 (control) or PA28γ-knockdown (PA28γ KD) cells together with or without HCV core protein. Cells were harvested at 48 h posttransfection, and nuclear extracts were mixed with the reaction buffer for EMSA. (*Upper*) The resulting mixtures were subjected to PAGE and blotted with horseradish peroxidase-streptavidin. The mobility shift of the LXRE probe is indicated by an arrow. (*Lower*) Expression of HCV core, HA-RXRα, FLAG-LXRα, and PA28γ in cells was detected by immunoblotting. (*B*) Effect of PA28γ knockout on the LXRα/RXRα–DNA complex in the mouse liver. (*Upper*) Nuclear extracts were prepared from the livers of 2-month-old PA28$\gamma^{-/-}$, PA28$\gamma^{+/+}$CoreTg, PA28$\gamma^{-/-}$CoreTg, and PA28$\gamma^{+/+}$ mice and subjected to EMSA. The mobility shift of the LXRE probe is indicated by an arrow. (*Lower*) The expression of HCV core, PA28γ, and β-actin in the livers of the mice was detected by immunoblotting. (*C*) Effect of HCV core protein on *srebp-1* promoter activity in PA28γ-knockout fibroblasts. A plasmid encoding firefly luciferase under the control of the *srebp-1c* promoter was transfected into MEFs prepared from PA28$\gamma^{+/+}$ (*Left*) or PA28$\gamma^{-/-}$ (*Right*) mice together with a plasmid encoding a *Renilla* luciferase. An empty plasmid or plasmids encoding mouse RXRα or LXRα were also cotransfected into the cells together with (gray bars) or without (white bars) a plasmid encoding HCV core protein. Luciferase activity under the control of the *srebp-1c* promoter was determined, and it is expressed as the fold increase in relative luciferase activity after standardization with the activity of *Renilla* luciferase.

tiates *srebp-1c* promoter activity in an LXRα/RXRα-dependent manner.

HCV Core Protein Activates the *srepb-1c* Promoter in an LXRα/RXRα- and PA28γ-Dependent Manner. To examine whether PA28γ is required for HCV core-induced enhancement of *srebp-1c* promoter activity in human liver cells, a PA28γ-knockdown human hepatoma cell line (FLC4 KD) was prepared. Enhancement of binding of the LXRE probe to LXRα/RXRα by coexpression of HCV core protein and LXRα/RXRα in FLC4 cells was diminished by knockdown of the PA28γ gene (Fig. 5*A*). Furthermore, formation of the LXRα/RXRα–LXRE complex was enhanced in the livers of PA28$\gamma^{+/+}$CoreTg mice but not in those of PA28$\gamma^{-/-}$, PA28$\gamma^{+/+}$, or PA28$\gamma^{-/-}$CoreTg mice (Fig. 5*B*). The expression of the HCV core protein in the mouse embryonic fibroblasts (MEFs) of PA28$\gamma^{+/+}$ mice induced the activation of the mouse *srebp-1c* promoter through the endogenous expression of LXRα and RXRα (Fig. 5*C Left*). Further enhancement of the activation of the *srebp-1c* promoter by HCV core protein in PA28$\gamma^{+/+}$ MEFs was achieved by the exogenous expression of both LXRα and RXRα. However, no enhancing effect of HCV core protein on *srebp-1c* promoter activity was observed in PA28$\gamma^{-/-}$ MEFs (Fig. 5*C Right*). These results support the notion that HCV core protein enhances the activity of the *srepb-1c* promoter in an LXRα/RXRα- and PA28γ-dependent manner.

Table 1. HCC in mice at 16–18 months of age

Mouse and sex	Total no. of mice	No. of mice developing HCC	Incidence, %
PA28$\gamma^{+/+}$CoreTg			
Male	17	5	29.4
Female	28	3	10.7
PA28$\gamma^{+/-}$			
Male	16	0	0
Female	4	0	0
PA28$\gamma^{-/-}$			
Male	23	0	0
Female	13	0	0
PA28$\gamma^{-/-}$CoreTg			
Male	15	0	0
Female	21	0	0

PA28γ Plays a Crucial Role in the Development of HCC in PA28$\gamma^{+/+}$ CoreTg Mice. The incidence of hepatic tumors in male PA28$\gamma^{+/+}$ CoreTg mice older than 16 months was significantly higher than that in age-matched female PA28$\gamma^{+/+}$CoreTg mice (6). We reconfirmed here that the incidence of HCC in male and female PA28$\gamma^{+/+}$CoreTg mice at 16–18 months of age was 29.4% (5 of 17 mice) and 10.7% (3 of 28 mice), respectively. To our surprise, however, no HCC developed in PA28$\gamma^{-/-}$CoreTg mice (males, 15; females, 21), although, as expected, no HCC was observed in PA28$\gamma^{+/-}$ (males, 16; females, 4) and PA28$\gamma^{-/-}$ mice (males, 23; females, 13) (Table 1). These results clearly indicate that PA28γ plays an indispensable role in the development of HCC induced by HCV core protein.

Discussion

HCV core protein is detected in the cytoplasm and partially in the nucleus and mitochondria of culture cells and hepatocytes of transgenic mice and hepatitis C patients (6, 23, 24, 26). Degradation of HCV core protein was enhanced by deletion of the C-terminal transmembrane region through a ubiquitin/proteasome-dependent pathway (27). We previously reported (18) that PA28γ binds directly to HCV core protein and then enhances degradation of HCV core protein in the nucleus through a proteasome-dependent pathway because HCV core protein was accumulated in nucleus of human cell line by treatment with proteasome inhibitor MG132. In this work, accumulation of HCV core protein was observed in nucleus of hepatocytes of PA28$\gamma^{-/-}$CoreTg mice (Fig. 1*D*). This result directly demonstrates that HCV core protein migrates into the nucleus and is degraded through a PA28γ-dependent pathway. However, HCV core protein accumulated in the nucleus because knockout of PA28γ gene abrogated the ability to cause liver pathology, suggesting that interaction of HCV core protein with PA28γ in the nucleus is prerequisite for the liver pathology induced by HCV core protein. We have previously shown (18) that HCV core protein is degraded through a PA28γ-dependent pathway, and Minami *et al.* (28) reported that PA28γ has a cochaperone activity with Hsp90. Therefore, degradation products of HCV core protein by means of PA28γ-dependent processing or correct folding of HCV core protein through cochaperone activity of PA28γ might be involved in the development of liver pathology. We do not know the reason why knockout of the PA28γ gene does not affect the total amount of HCV core protein in the liver of the transgenic mice. PA28γ-dependent degradation of HCV core protein may be independent of ubiquitination, as shown in SRC-3 (21), whereas knockdown of PA28γ in a human hepatoma cell line enhanced the ubiquitination of HCV core protein [supporting information (SI) Fig. 6], suggesting that lack of PA28γ suppresses a ubiquitin-independent degradation but enhances a ubiquitin-dependent degradation of HCV core protein. Therefore, the total amount of HCV

core protein in the liver of the mice may be unaffected by the knockout of the PA28γ gene.

Our results suggest that the interaction of HCV core protein with PA28γ leads to the activation of the *srebp-1c* promoter along an LXRα/RXRα-dependent pathway and the development of liver steatosis and HCC. HCV core protein was not included in the LXRα/RXRα–LXRE complex (Fig. 3*A*), suggesting that HCV core protein indirectly activates the *srebp-1c* promoter. Cytoplasmic HCV core protein was shown to interact with Sp110b, which is a transcriptional corepressor of RARα-dependent transcription, and this interaction leads to the sequestering of Sp110b in the cytoplasm, resulting in the activation of RARα-dependent transcription (29). The sequestration of an unidentified corepressor of the LXRα/RXRα heterodimer in the cytoplasm by HCV core protein may also contribute to the activation of the *srebp-1c* promoter. Although the precise physiological function of PA28γ-proteasome activity in the nucleus is not known, PA28γ has previously been shown (21) to regulate nuclear hormone receptors by means of the degradation of its coactivator SRC-3 and to participate in the fully Hsp90-dependent protein refolding (28). It appears reasonable to speculate that degradation or refolding of HCV core protein in a PA28γ-dependent pathway might be involved in the modulation of transcriptional regulators of various promoters, including the *srebp-1c* promoter. Saturated or monounsaturated fatty acids have been shown to enhance HCV RNA replication in Huh7 cells containing the full-length HCV replicon (7). The up-regulation of fatty acid biosynthesis by HCV core protein may also contribute to the efficient replication of HCV and to the progression of HCV pathogenesis.

Expression of HCV core protein was reported to enhance production of reactive oxygen species (ROS) (30), which leads to carbonylation of intracellular proteins (31). Enhancement of ROS production may trigger double-stranded DNA breaks and result in the development of HCC (30, 32, 33). HCV core protein could enhance the protein carbonylation in the liver of the transgenic mice in the presence but not in the absence of PA28γ (SI Fig. 7), suggesting that PA28γ is required for ROS production induced by HCV core protein. Development of HCC was observed in PA28γ$^{+/+}$CoreTg mice but not in PA28γ$^{-/-}$CoreTg mice (Table 1). Enhancement of ROS production by HCV core protein in the presence of PA28γ might be involved in the development of HCC in PA28γ$^{+/+}$CoreTg mice.

It is well known that resistant viruses readily emerge during the treatment with antiviral drugs targeting the viral protease or replicase, especially in the case of infection with RNA viruses. Therefore, antivirals targeting the host factors that are indispensable for the propagation of viruses might be an ideal target for the development of antiviral agents because of a lower rate of mutation than that of viral genome, if they have no side effects to patients. Importantly, the amino acid sequence of PA28γ of mice is identical to that of human, and mouse PA28γ is dispensable because PA28γ knockout mice exhibit no abnormal phenotype except for mild growth retardation. Therefore, PA28γ might be a promising target for an antiviral treatment of chronic hepatitis C with negligible side effects.

In summary, we observed that a knockout of the PA28γ gene from PA28γ$^{+/+}$CoreTg mice induced the accumulation of HCV core protein in the nucleus and disrupted the development of both steatosis and HCC. Activation of the *srebp-1c* promoter was up-regulated by HCV core protein both *in vitro* and *in vivo* through a PA28γ-dependent pathway, suggesting that PA28γ plays a crucial role in the development of liver pathology induced by HCV infection.

Materials and Methods

Histology and immunohistochemistry, real-time PCR, and detection of proteins modified by ROS are discussed in *SI Materials and Methods*.

Plasmids and Reagents. Human PA28γ cDNA was isolated from a human fetal brain library (18). The gene encoding HCV core protein was amplified from HCV strain J1 (genotype 1b) (34) and cloned into pCAG-GS (35). Mouse cDNAs of RXRα and LXRα were amplified by PCR from the total cDNAs of the mouse liver. The RXRα and LXRα genes were introduced into pEF-FLAGGspGBK (36) and pcDNA3.1 (Invitrogen, Carlsbad, CA), respectively. The targeting fragment for human PA28γ knockdown (GGATCCGGTGGATCAGGAAGTGAAGTTCAAGAGA-CTTCACTTCCTGATCCACCTTTTTTGGAAAAGCTT) was introduced into the BamHI and HindIII sites of pSilencer 4.1 U6 hygro vector (Ambion, Austin, TX). Mouse anti-FLAG (M2) and mouse anti-β-actin antibodies were purchased from Sigma (St. Louis, MO). Rabbit polyclonal antibody against synthetic peptides corresponding to amino acids 70–85 of PA28γ was obtained from AFFINITI (Exeter, U.K.). Horseradish peroxidase-conjugated goat anti-mouse and anti-rabbit IgGs were purchased from ICN Pharmaceuticals (Aurora, OH). Rabbit anti-HCV core protein was prepared by immunization with recombinant HCV core protein (amino acids 1-71), as described in ref. 24. Mouse monoclonal antibody to HCV core protein was kindly provided by S. Yagi (37). The plasmid for expression of HA-tagged ubiquitin was described in ref. 27.

Preparation of PA28γ-Knockout HCV CoreTg Mice. The generation of C57BL/6 mice carrying the gene encoding HCV core protein genotype 1b line C49 and that of PA28γ$^{-/-}$ mice have been reported previously (22, 25). Both strains were crossbred with each other to create PA28γ$^{-/-}$CoreTg mice. PA28γ$^{-/-}$CoreTg mice were identified by PCR targeted at the PA28γ or HCV core gene (22, 25). Using 1 μg of genomic DNA obtained from the mouse tail, the PA28γ gene was amplified by PCR with the following primers: sense, PA28-3 (AGGTGGATCAGGAAGTGAAGCTCAA); and antisense, PA28γ-5cr (CACCTCACTTGTGATCCGCTCTCT-GAAAGAATCAACC). The targeted sequence for the PA28γ-knockout mouse was detected by PCR using the PA28-3 primer and the PAKO-4 primer (TGCAGTTCATTCAGGGCACCGGA-CAG). The transgene encoding HCV core protein was detected by PCR as described in ref. 25. The expression of PA28γ and HCV core protein in the livers of 6-month-old mice was confirmed by Western blotting with mouse monoclonal antibody to HCV core protein, clone 11-10, and rabbit antibody to PA28γ. Mice were cared for according to the institutional guidelines. The mice were given ordinary feed, CRF-1 (Charles River Laboratories, Yokohama, Japan), and they were maintained under specific pathogen-free conditions.

All animal experiments conformed to the Guidelines for the Care and Use of Laboratory Animals, and they were approved by the Institutional Committee of Laboratory Animal Experimentation (Research Institute for Microbial Diseases, Osaka University).

Preparation of Mouse Embryonic Fibroblasts. MEFs were prepared as described in ref. 22. MEFs were cultured at 37°C under an atmosphere of 5% CO_2 in Dulbecco's modified Eagle's medium (Sigma) supplemented with 10% FBS, penicillin, streptomycin, sodium pyruvate, and nonessential amino acids.

Transfection and Immunoblotting. Plasmid vectors were transfected into the MEFs and 293T cells by liposome-mediated transfection by using Lipofectamine 2000 (Invitrogen). The amount of HCV core protein in the liver tissues was determined by an ELISA as described in ref. 37. The cell lysates were subjected to SDS/PAGE (12.5% gel), and they were then transferred onto PVDF membranes. Proteins on the membranes were treated with specific antibody and Super Signal Femto (Pierce, Rockford, IL). The results were then visualized by using an LAS3000 imaging system (Fuji Photo Film, Tokyo, Japan). The method of immunoprecipitation test is described in ref. 18.

Reporter Assay for *srebp-1c* Promoter Activity. The genomic DNA fragment encoding the *srebp-1c* promoter region (located from residues −410 to +24) was amplified from a mouse genome. The fragment was introduced into the KpnI and HindIII sites of pGL3-Basic (Promega, Madison, WI), and it was designated as pGL3-srebp-1cPro. The plasmids encoding RXRα and LXRα were transfected into MEFs together with pGL3-srebp-1cPro and a control plasmid encoding *Renilla* luciferase (Promega). The total DNA for transfection was normalized by the addition of empty plasmids. Cells were harvested at 24 h posttransfection. The ligand of RXRα, 9-*cis*-retinoic acid (Sigma), and that of LXRα, 22(*R*)-hydroxylcholesterol (Sigma) were added at a final concentration of 5 μM each to the culture medium of 293T cells transfected with pGL3-srebp-1cPro together with expression plasmids encoding RXRα, LXRα, and HCV core protein at 24 h posttransfection. Cells were harvested 24 h after treatment. Luciferase activity was measured by using the dual-luciferase reporter assay system (Promega). Firefly luciferase activity was standardized with that of *Renilla* luciferase, and the results are expressed as the fold increase in relative luciferase units.

Electrophoresis Mobility Shift Assay (EMSA). EMSA was carried out by using a LightShift Chemiluminescent EMSA kit (Pierce) according to the manufacturer's protocol. Nuclear extract of the cell lines and liver tissue was prepared with an NE-PER nuclear and cytoplasmic extraction reagent kit (Pierce). Briefly, double-stranded oligonucleotides for EMSA were prepared by annealing both strands of each LXRE of the *srebp-1c* promoter (5′-GGACGCCCGCTAGTAACCCCGGC-3′) (16). Both strands were labeled at the 5′ ends with biotin. The annealed probe was incubated for 20 min on ice with nuclear extract (3 μg of protein) in a reaction buffer containing 10 mM Tris·HCl (pH 7.5), 50 mM KCl, 1 mM DTT, 0.05 μg/μl poly(dI-dC), 2.5% glycerol, 0.05% Nonidet P-40, and 0.1 nM labeled probe, with or without 1 mM nonlabeled probe. The resulting mixture was subjected to PAGE (5% gel) at 120 V for 30 min in 0.5× TBE. The DNA–protein complex was transferred to a Hybond N+ membrane (Amersham, Piscataway, NJ), incubated with horseradish peroxidase-conjugated streptavidin, and visualized by using an LAS3000 imaging system.

Statistical Analysis. The results are expressed as the mean ± SD. The significance of differences in the means was determined by Student's *t* test.

We thank H. Murase for secretarial work and D. C. S. Huang for providing the plasmids. This work was supported in part by grants-in-aid from the Ministry of Health, Labor, and Welfare; the Ministry of Education, Culture, Sports, Science, and Technology; the 21st Century Center of Excellence Program; and the Foundation for Biomedical Research and Innovation.

1. Wasley A, Alter MJ (2000) *Semin Liver Dis* 20:1–16.
2. Bach N, Thung SN, Schaffner F (1992) *Hepatology* 15:572–577.
3. Lefkowitch JH, Schiff ER, Davis GL, Perrillo RP, Lindsay K, Bodenheimer HC, Jr., Balart LA, Ortego TJ, Payne J, Dienstag JL, *et al.* (1993) *Gastroenterology* 104:595–603.
4. Barba G, Harper F, Harada T, Kohara M, Goulinet S, Matsuura Y, Eder G, Schaff Z, Chapman MJ, Miyamura T, Brechot C (1997) *Proc Natl Acad Sci USA* 94:1200–1205.
5. Hope RG, McLauchlan J (2000) *J Gen Virol* 81:1913–1925.
6. Moriya K, Fujie H, Shintani Y, Yotsuyanagi H, Tsutsumi T, Ishibashi K, Matsuura Y, Kimura S, Miyamura T, Koike K (1998) *Nat Med* 4:1065–1067.
7. Kapadia SB, Chisari FV (2005) *Proc Natl Acad Sci USA* 102:2561–2566.
8. Su AI, Pezacki JP, Wodicka L, Brideau AD, Supekova L, Thimme R, Wieland S, Bukh J, Purcell RH, Schultz PG, Chisari FV (2002) *Proc Natl Acad Sci USA* 99:15669–15674.
9. Wang C, Gale M, Jr, Keller BC, Huang H, Brown MS, Goldstein JL, Ye J (2005) *Mol Cell* 18:425–434.
10. Horton JD, Shimomura I, Brown MS, Hammer RE, Goldstein JL, Shimano H (1998) *J Clin Invest* 101:2331–2339.
11. Pai JT, Guryev O, Brown MS, Goldstein JL (1998) *J Biol Chem* 273:26138–26148.
12. Shimano H, Horton JD, Hammer RE, Shimomura I, Brown MS, Goldstein JL (1996) *J Clin Invest* 98:1575–1584.
13. Shimano H, Horton JD, Shimomura I, Hammer RE, Brown MS, Goldstein JL (1997) *J Clin Invest* 99:846–854.
14. Shimano H, Shimomura I, Hammer RE, Herz J, Goldstein JL, Brown MS, Horton JD (1997) *J Clin Invest* 100:2115–2124.
15. Repa JJ, Liang G, Ou J, Bashmakov Y, Lobaccaro JM, Shimomura I, Shan B, Brown MS, Goldstein JL, Mangelsdorf DJ (2000) *Genes Dev* 14:2819–2830.
16. Yoshikawa T, Shimano H, Amemiya-Kudo M, Yahagi N, Hasty AH, Matsuzaka T, Okazaki H, Tamura Y, Iizuka Y, Ohashi K, *et al.* (2001) *Mol Cell Biol* 21:2991–3000.
17. Tsutsumi T, Suzuki T, Shimoike T, Suzuki R, Moriya K, Shintani Y, Fujie H, Matsuura Y, Koike K, Miyamura T (2002) *Hepatology* 35:937–946.
18. Moriishi K, Okabayashi T, Nakai K, Moriya K, Koike K, Murata S, Chiba T, Tanaka K, Suzuki R, Suzuki T, *et al.* (2003) *J Virol* 77:10237–10249.
19. Masson P, Andersson O, Petersen UM, Young P (2001) *J Biol Chem* 276:1383–1390.
20. Li J, Rechsteiner M (2001) *Biochimie* 83:373–383.
21. Li X, Lonard D, Jung SY, Malovannaya A, Feng Q, Qin J, Tsai SY, Tsai M, O'Malley BW (2006) *Cell* 124:381–392.
22. Murata S, Kawahara H, Tohma S, Yamamoto K, Kasahara M, Nabeshima Y, Tanaka K, Chiba T (1999) *J Biol Chem* 274:38211–38215.
23. Falcon V, Acosta-Rivero N, Chinea G, Gavilondo J, de la Rosa MC, Menendez I, Duenas-Carrera S, Vina A, Garcia W, Gra B, *et al.* (2003) *Biochem Biophys Res Commun* 305:1085–1090.
24. Suzuki R, Sakamoto S, Tsutsumi T, Rikimaru A, Tanaka K, Shimoike T, Moriishi K, Iwasaki T, Mizumoto K, Matsuura Y, *et al.* (2005) *J Virol* 79:1271–1281.
25. Moriya K, Yotsuyanagi H, Shintani Y, Fujie H, Ishibashi K, Matsuura Y, Miyamura T, Koike K (1997) *J Gen Virol* 78:1527–1531.
26. Yasui K, Wakita T, Tsukiyama-Kohara K, Funahashi SI, Ichikawa M, Kajita T, Moradpour D, Wands JR, Kohara M (1998) *J Virol* 72:6048–6055.
27. Suzuki R, Tamura K, Li J, Ishii K, Matsuura Y, Miyamura T, Suzuki T (2001) *Virology* 280:301–309.
28. Minami Y, Kawasaki H, Minami M, Tanahashi N, Tanaka K, Yahara I (2000) *J Biol Chem* 275:9055–9061.
29. Watashi K, Hijikata M, Tagawa A, Doi T, Marusawa H, Shimotohno K (2003) *Mol Cell Biol* 23:7498–7509.
30. Machida K, Cheng KT, Lai CK, Jeng KS, Sung VM, Lai MM (2006) *J Virol* 80:7199–7207.
31. Nystrom T (2005) *EMBO J* 24:1311–1317.
32. Bromberg JF, Wrzeszczynska MH, Devgan G, Zhao Y, Pestell RG, Albanese C, Darnell JE, Jr (1999) *Cell* 98:295–303.
33. Carballo M, Conde M, El Bekay R, Martín-Nieto J, Camacho MJ, Monteseirin J, Conde J, Bedoya FJ, Sobrino F (1999) *J Biol Chem* 274:17580–17586.
34. Aizaki H, Aoki Y, Harada T, Ishii K, Suzuki T, Nagamori S, Toda G, Matsuura Y, Miyamura T (1998) *Hepatology* 27:621–627.
35. Niwa H, Yamamura K, Miyazaki J (1991) *Gene* 108:193–199.
36. Huang DC, Cory S, Strasser A (1997) *Oncogene* 14:405–414.
37. Aoyagi K, Ohue C, Iida K, Kimura T, Tanaka E, Kiyosawa K, Yagi S (1999) *J Clin Microbiol* 37:1802–1808.

JOURNAL OF VIROLOGY, Sept. 2007, p. 8953–8966 Vol. 81, No. 17
0022-538X/07/$08.00+0 doi:10.1128/JVI.00649-07

Hepatitis C Virus Nonstructural Protein 5A Modulates the Toll-Like Receptor-MyD88-Dependent Signaling Pathway in Macrophage Cell Lines▽

Takayuki Abe,[1] Yuuki Kaname,[1] Itsuki Hamamoto,[1]† Yoshimi Tsuda,[1]‡ Xiaoyu Wen,[1] Shuhei Taguwa,[1] Kohji Moriishi,[1] Osamu Takeuchi,[2] Taro Kawai,[2] Tatsuya Kanto,[3,4] Norio Hayashi,[3] Shizuo Akira,[2] and Yoshiharu Matsuura[1]*

Department of Molecular Virology,[1] and Department of Host Defense,[2] Research Institute for Microbial Diseases, and Department of Gastroenterology and Hepatology,[3] and Department of Dendritic Cell Biology and Clinical Applications,[4] Graduate School of Medicine, Osaka University, Osaka, Japan

Received 27 March 2007/Accepted 6 June 2007

Hepatitis C virus (HCV) infection induces a wide range of chronic liver injuries; however, the mechanism through which HCV evades the immune surveillance system remains obscure. Blood dendritic cells (DCs) play a pivotal role in the recognition of viral infection and the induction of innate and adaptive immune responses. Several reports suggest that HCV infection induces the dysfunction of DCs in patients with chronic hepatitis C. Toll-like receptor (TLR) has been shown to play various roles in many viral infections; however, the involvement of HCV proteins in the TLR signaling pathway has not yet been precisely elucidated. In this study, we established mouse macrophage cell lines stably expressing HCV proteins and determined the effect of HCV proteins on the TLR signaling pathways. Immune cells expressing NS3, NS3/4A, NS4B, or NS5A were found to inhibit the activation of the TLR2, TLR4, TLR7, and TLR9 signaling pathways. Various genotypes of NS5A bound to MyD88, a major adaptor molecule in TLR, inhibited the recruitment of interleukin-1 receptor-associated kinase 1 to MyD88, and impaired cytokine production in response to TLR ligands. Amino acid residues 240 to 280, previously identified as the interferon sensitivity-determining region (ISDR) in NS5A, interacted with the death domain of MyD88, and the expression of a mutant NS5A lacking the ISDR partially restored cytokine production. These results suggest that the expression of HCV proteins modulates the TLR signaling pathway in immune cells.

Hepatitis C virus (HCV) belongs to the family *Flaviviridae* and possesses a positive, single-stranded RNA genome that encodes a single polyprotein composed of approximately 3,000 amino acids. HCV polyprotein is processed by host and viral proteases, resulting in 10 viral proteins. Viral structural proteins, including the capsid protein and two envelope proteins, are located in the N-terminal one-third of the polyprotein, followed by nonstructural proteins. HCV infects 170 million people worldwide and frequently leads to cirrhosis and hepatocellular carcinoma (36). In over one-half of patients, acute infection evolves into a persistent carrier state, presumably due to the ability of HCV to incapacitate the activation of the host immune mechanisms. Dendritic cells (DCs) are one type of potent antigen-presenting cell in vivo and play a crucial role in the enhancement and regulation of cell-mediated immune reactions. Since DCs express various costimulatory and/or adhesion molecules, they can activate even naïve T cells in a primary response. The role of the response of HCV antigen-specific T cells in viral clearance or persistence has been investigated extensively in both humans and chimpanzees (6, 27, 48, 51). These studies suggest that acute HCV infections followed by viral clearance are associated with a high frequency of HCV-specific $CD4^+$ and $CD8^+$ T-cell responses that can persist (27, 51), while chronic HCV infections are characterized by weak and restricted $CD4^+$ and $CD8^+$ T-cell responses that are not sustained (51).

Toll-like receptors (TLRs) are membrane-bound receptors that can be activated by the binding of molecular structures conserved among families of microbes. More than 10 different TLRs have been identified to date (2). They are highly conserved among mammals and are expressed in a variety of cell types. TLR binding and stimulation by pathogen-associated molecules is followed by a cascade of intracellular events that culminate in the expression of multiple genes (2). TLR signaling is mediated primarily by the adaptor protein myeloid differentiation factor 88 (MyD88), which triggers the activation of transcription factors, such as NF-κB, that are essential for the expression of proinflammatory cytokine genes (2). This pathway also leads to the potent production of type I interferon (IFN) through the activation of IFN regulatory factor 7 (IRF7) upon stimulation of TLR7 or TLR9 (22). In contrast, Toll/interleukin-1 (IL-1) receptor homology domain-containing adaptor-inducing IFN-β (TRIF/TICAM-1) mediates the production of type I IFNs primarily through the activation of IRF3 in response to TLR3 or TLR4 stimulation (2). Type I IFN induces the maturation of DCs by increasing both the expression of costimulatory molecules such as CD80, CD86, and CD40 and antigen presentation via major histocompatibility

* Corresponding author. Mailing address: Research Center for Emerging Infectious Diseases, Research Institute for Microbial Diseases, Osaka University, 3-1 Yamada-oka, Suita, Osaka 565-0871, Japan. Phone: 81-6-6879-8340. Fax: 81-6-6879-8269. E-mail: matsuura@biken.osaka-u.ac.jp.
† Present address: Infectious Disease Surveillance Center, National Institute of Infectious Diseases, Tokyo, Japan.
‡ Present address: Department of Disease Control, Graduate School of Veterinary Medicine, Hokkaido University, Sapporo 060-0818, Japan.
▽ Published ahead of print on 13 June 2007.

complex class I in addition to classical endogenous antigen presentation; it also facilitates the cross-presentation of viral antigens. A cumulative report has shown that DC activation via TLR signaling is a prerequisite for the subsequent induction of vigorous T-cell responses (42). Some viral proteins have been shown to inhibit the TLR-dependent signaling pathway through interactions with the downstream adaptor molecules, suggesting that the alteration of TLR-mediated signals is one of the mechanisms of virus-induced immune modulation (49). Dysfunction of DCs in patients with chronic HCV infection due to immaturation caused by the direct infection of DCs by HCV or by interactions with HCV proteins has been reported previously (4, 21). On the other hand, there have also been contrasting reports suggesting a lack of impairment of DC function in both chimpanzees and humans chronically infected with HCV (26, 32). Thus, at present, alterations in the TLR signaling pathway in the immune cells of patients with chronic hepatitis C virus infection are not well understood.

In the present study, we examined the effect of HCV proteins on TLR function in murine macrophage cell lines stably expressing HCV proteins. The expression of NS3, NS3/4A, NS4B, or NS5A was found to impair the activation of the TLR signaling pathways, and NS5A interacted with MyD88 through the IFN sensitivity-determining region (ISDR) and impaired cytokine production. To the best of our knowledge, this is the first demonstration of NS5A as an immunomodulator of TLR signaling pathways through the direct interaction with an adaptor molecule in immune cells.

MATERIALS AND METHODS

Cell culture. Human embryonic kidney 293T cells and mouse macrophage RAW264.7 cells were maintained in Dulbecco's modified Eagle's medium (Sigma, St. Louis, MO) containing 10% fetal calf serum. All cells were cultured at 37°C in a humidified atmosphere with 5% CO_2.

Plasmids and viruses. DNA fragments encoding each of the HCV structural and nonstructural proteins were generated from a full-length cDNA clone of genotype 1b strain J1 (1) by PCR using *Pfu* Turbo DNA polymerase (Stratagene, La Jolla, CA). The fragments were cloned into pCAGGs-puro/N-Flag, in which the sequence encoding a Flag tag is inserted at the 5′ terminus of the cloning site of pCAGGs-puro (37). A protease-deficient NS3/4A mutant with Ser^{139} replaced with Ala (S139A) was generated by the method of splicing by overlap extension and cloned into pCAGGs-puro. NS5A genes were amplified by PCR from HCV clones of strains of J1 (genotype 1b), H77c (genotype 1a, kindly provided by J. Bukh), and JFH1 (genotype 2a, kindly provided by T. Wakita) and cloned into pcDNA3.1Flag/HA (38). The NS5A deletion mutants were prepared as described previously (16). DNA fragments encoding a human MyD88, human Toll–IL-1 receptor domain-containing adapter protein (TIRAP), and human TRIF-related adapter molecule (TRAM) were amplified by reverse transcription-PCR from total RNA of THP-1 cells and cloned into pcDNA3.1-C-Myc-His (Invitrogen, Carlsbad, CA) and pcDNA3.1Flag/HA. Murine IPS-1 (mIPS-1) was amplified from total RNA of RAW264.7 cells by reverse transcription-PCR and cloned into pcDNA3.1Flag/HA. Human MyD88 deletion mutants and a mIPS-1 mutant with Cys^{508} replaced by Ala (C508A) were generated by the method of splicing by overlap extension and cloned into pcDNA3.1Flag/HA. pCMVIRAK1-myc and pCMVIRAK4-myc, encoding IL-1 receptor-associated kinase 1 (IRAK-1) and IRAK-4, respectively, were prepared as described previously (53). pEFBossTICAM-I-HA was kindly provided by T. Seya (44). All PCR products were confirmed by sequencing by using an ABI PRSM 310 genetic analyzer (Applied Biosystems, Tokyo, Japan). Vesicular stomatitis virus (VSV) (Indiana strain, NCP12.1) (19) was kindly provided by M. A. Whitt.

Establishment of stable cell lines expressing HCV proteins. pCAGGs-puro/N-Flag plasmids encoding HCV proteins were transfected into RAW264.7 cells by liposome-mediated transfection using Lipofectamine 2000 (Invitrogen) and selected with 10 μg/ml of puromycin (InvivoGen, San Diego, CA). After about 2 to 3 weeks of selection, several clones were isolated, and cell lysates of each clone were immunoblotted with each of specific mouse anti-HCV antibody (1) or anti-Flag M2 mouse monoclonal antibody (Sigma). Macrophage cell lines stably expressing HCV proteins and a control cell line obtained by transfection with an empty pCAGGs-puro vector were maintained in the presence of puromycin (10 μg/ml) throughout the experiments.

Immunoprecipitation and immunoblotting. Cells were seeded onto a six-well tissue culture plate 24 h before transfection. The plasmids were transfected by the lipofection method, and the cells were harvested at 48 h posttransfection, washed three times with 1 ml of ice-cold phosphate-buffered saline (PBS), and suspended in 0.4 ml lysis buffer containing 20 mM Tris-HCl (pH 7.4), 135 mM NaCl, 1% Triton X-100, 10% glycerol, and protease inhibitor cocktail tablets (Roche Molecular Biochemicals, Mannheim, Germany). Cell lysates were incubated for 30 min at 4°C and centrifuged at 14,000 × *g* for 15 min at 4°C. The supernatant was immunoprecipitated with 1 μg of mouse monoclonal anti-Flag M2, anti-hemagglutinin (HA) 16B12 (HA.11; BabCO, Richmond, CA), or anti-hexahistidine (Santa Cruz Biotechnology, Santa Cruz, CA) antibody and 10 μl of protein G-Sepharose 4B Fast Flow beads (Amersham Pharmacia Biotech, Franklin Lakes, NJ) at 4°C for 90 min. The immunocomplex was precipitated with the beads by centrifugation at 5,000 × *g* for 1 min and then washed five times with 0.4 ml of 20 mM Tris-HCl (pH 7.4) containing 135 mM NaCl and 0.05% Tween 20 (TBST buffer) by centrifugation. The proteins binding to the beads were boiled in 20 μl of sample buffer and then subjected to sodium dodecyl sulfate–12.5% polyacrylamide gel electrophoresis and transferred onto polyvinylidene difluoride membranes (Millipore, Tokyo, Japan). The membranes were blocked with TBST containing 5% skim milk at room temperature for 1 h; incubated with mouse monoclonal anti-Flag M2, anti-HA 16B12, or anti-hexahistidine monoclonal antibody at room temperature for 1 h; and then incubated with horseradish peroxidase-conjugated anti-mouse immunoglobulin G (IgG) antibody at room temperature for 1 h. The cell lines (2×10^6 cells/well) were stimulated with various doses of lipopolysaccharide (LPS) derived from *Salmonella enterica* serovar Minnesota (Re-595) (Sigma), peptidoglycans (PGN) derived from *Staphylococcus aureus* (Sigma), R-837 (InvivoGen), or phosphorothioate-stabilized mouse CpG (mCpG) oligodeoxynucleotides (ODN1668) (TCC-ATG-ACG-TTC-CTG-ATG-CT) (Invitrogen) for the times indicated, and the phosphorylation status of extracellular signal-regulated kinase (ERK) was determined by immunoblotting using antibodies specific to ERK1/2 or phosphorylated ERK1/2 (T202/Y204) (Cell Signaling Technology, Inc., Beverly, MA). Cells (1×10^6 cells/well) were treated with various doses of mouse IFN-α (PBL Biomedical Laboratories, New Brunswick, NJ) or VSV for 24 h, and the phosphorylation status of double-stranded RNA-dependent protein kinase (PKR) and signal transducer and activator of transcription 1 (STAT1) was determined by immunoblotting using antibodies specific to STAT1 (Cell Signaling), phosphorylated STAT1 (Cell Signaling), or phosphorylated PKR (BioSource International, Inc., Camarillo, CA). The immune complexes were visualized with Super Signal West Femto substrate (Pierce, Rockford, IL) and detected by using an LAS-3000 image analyzer system (Fujifilm, Tokyo, Japan).

Cytokine production and enzyme-linked immunosorbent assay (ELISA). To evaluate cytokine production in macrophage cell lines expressing HCV proteins, cells were seeded onto 96-well plates at a concentration of 1×10^5 cells/well and stimulated with various doses of LPS, PGN, R-837, or mCpG. After 24 h of incubation, culture supernatants were collected, and IL-6 production was determined by using an OptEIA mouse IL-6 set purchased from BD Pharmingen (San Diego, CA).

Real-time PCR. The cell lines (3×10^6 cells/well) were stimulated with R-837, LPS, PGN, mCpG, VSV, and polyinosine-poly(C) [poly(I:C)] (Invivogen) for the times indicated, and the expression of mRNA of cytokines, chemokines, and TLR genes was determined by real-time PCR. Total RNA was prepared from the macrophage cell lines using an RNeasy Mini kit (QIAGEN). First-strand cDNA was synthesized using a ReverTra Ace (TOYOBO, Japan) and oligo$(dT)_{20}$ primer. Each cDNA was estimated by Platinum SYBR Green qPCR SuperMix UDG (Invitrogen) according to the manufacturer's protocol. Fluorescent signals were analyzed by using an ABI PRISM 7000 apparatus (Applied Biosystems). Mouse Ccl2, IFN-β, IFN-α1, IFN-α4, and IL-1-α genes were amplified with primer pairs 5′-GCATCCACGTGTTGGCTCA-3′ and 5′-CTCCAGCCTACTCATTGGGATCA-3′, 5′-ACACCAGCCTGGCTTCCATC-3′ and 5′-TTGGAGCTGGAGCTGCTTATAGTTG-3′, 5′-AGCCTTGACACTCCTGGTACAAATG-3′ and 5′-TGGGTCAGCTCACTCAGGACA-3′, 5′-GCTCAAGCCATCCTTGTGCTAA-3′ and 5′-CATTGAGCTGATGGAGGTC-3′, and 5′-TTGGTTAAATGACCTGCAACAGGA-3′ and 5′-AGGTCGGTCTCACTACCTGTGATG-3′, respectively. The mouse TLR2, TLR3, TLR4, TLR7, TLR9, and GAPDH (glyceraldehyde-3-phosphate dehydrogenase) genes were amplified using primer pairs 5′-AGCTCTTTGGCTCTTCTG-3′ and 5′-AGAACTGGGGGATATGC-3′, 5′-AAATCCTTGCGTTGCGAAGTG-3′ and 5′-TCAGTTGGGCGTTGTTCAAGAG-3′, 5′-GCCTCGAATCCTGAGCAAACA-3′ and 5′-CTTCTGCCCGGTAAGGTCCA-3′, 5′-TCTGCAGGAGCTCTGTCCTTGA-3′ and 5′-CAAGGCATGTCCTAGGTGGTGA-3′, 5′-ACCAATGGCACCCTGCCTAA-3′ and 5′-